2019•2020

Faculteit Industriële ingenieurswetenschappen

master in de industriële wetenschappen: bouwkunde

Masterthesis

A comparative study of the patch loading resistance of longitudinally stiffened girders

PROMOTOR :

Prof. dr. ir. Herve DEGEE

Stijn Janssens

Scriptie ingediend tot het behalen van de graad van master in de industriële wetenschappen: bouwkunde

Gezamenlijke opleiding UHasselt en KU Leuven

UHASSELT KU LEUVEN

UHASSELT KU LEUVEN

2019•2020

Faculteit Industriële ingenieurswetenschappen

master in de industriële wetenschappen: bouwkunde

Masterthesis

A comparative study of the patch loading resistance of longitudinally stiffened girders

PROMOTOR :

Prof. dr. ir. Herve DEGEE

Stijn Janssens

Scriptie ingediend tot het behalen van de graad van master in de industriële wetenschappen: bouwkunde

UHASSELT KU LEUVEN

Deze masterproef werd geschreven tijdens de COVID-19 crisis in 2020. Deze wereldwijde gezondheidscrisis heeft mogelijk een impact gehad op de opdracht, de onderzoekshandelingen en de onderzoeksresultaten.

Preface

Doing your master's thesis, be it abroad or at home, always is a unique and interesting experience. However, this year, it has proven to be extraordinary. During my first semester, I studied abroad at the Budapest University of Technology and Economics (BME), in the beautiful capital of Hungary. This is also where I met one of my promotors, Dr Balázs Kövesdi. Both Dr Kövesdi and my promotor at home, Prof Dr Ir Hervé Degée, are renowned figures in the field of, amongst others, steel applications. Now, in Budapest, there are a lot of bridges. Bridges can be manufactured out of various materials and built in several different ways. Steel bridges seemed like an obvious choice. Together, we decided on a broad subject: the patch loading resistance of longitudinally stiffened steel girders. During the academic year, the exact contents of the subject changed due to various circumstances. And while I might not see the initial subject ever get completed myself, I have been able to get a taste of what FEM software has to offer in praxis and how it compares to calculations according to the Eurocodes.

When it comes to realising this project, I would first and foremost like to thank Dr Balázs Kövesdi for giving me the initial push and introducing me to the whole topic, and Prof Dr Ir Hervé Degée for guiding me through it and expressing his feedback. I would also like to thank Ing Glenn van Vugt for the support he provided me whenever I encountered difficulties drawing the models in GiD and FINELG. Their help and knowledge aided me along the project.
Then I would like to thank my parents and my brother, Mathias, for their continued support and their efforts assisting me to collect the results.
Lastly, I would like to thank my girlfriend, Anne-Sofie, for always being there for me, for her patience, and for always believing in me.

Table of contents

List of tables

List of figures

List of symbols

The notations and symbols used in this thesis are described within this chapter. The symbols are listed in alphabetical order, Roman and Greek, respectively.

Roman notations and symbols

a	-	Length of the web panel
b_f	-	Width of the flange
b_l	-	Depth / Height of the upper panel
b_{st}	-	Width of the longitudinal stiffener
E	-	Modulus of elasticity, Young's modulus
f_u	-	Ultimate strength
f_y	-	Yield strength
f_{yf}	-	Yield strength of the flange
f_{yw}	-	Yield strength of the web
$f(s)$	-	Amplification factor for longitudinally stiffened webs
$f(s_s)$	-	Correction factor for the loaded length s_s
F	-	Force
F_{cr}	-	Elastic critical force for the relevant buckling mode based on the gross cross-sectional properties
F_y	-	Yield resistance
F_R	-	Predicted resistance for an unstiffened web
F_{Rd}	-	Design value of the predicted patch loading resistance
F_{Rl}	-	Predicted resistance for a longitudinally stiffened web according to an amplification factor model
h_l	-	Distance between the upper flange and the centre of gravity of the longitudinal stiffener
$h_{st,o}$	-	Outer height of the closed stiffener at the external (outer) side

$h_{st,w}$	-	Outer height of the closed stiffener at the internal (web) side
h_w	-	Depth / Height of the web
$h_{w,i}$	-	Depth / Height of a subpanel of the web; measured between a flange and a stiffener, or between two stiffeners
I_f	-	Moment of inertia of the flange
$I_{sl,1}$	-	Moment of inertia of the longitudinal stiffener closest to the loaded flange
k_F	-	Buckling coefficient
k_{sl}	-	Contribution of longitudinal stiffening to the buckling coefficient
l_y	-	Effective loaded length
m_1, m_2	-	Dimensionless parameters
s_s	-	Loaded length
s_y	-	Distance between the plastic hinges in a loaded flange
s_η	-	Modified distance between the outermost plastic hinges in a loaded flange
t_f	-	Thickness of the flange
t_i	-	Idealised flange thickness
t_{st}	-	Thickness of the stiffener
t_w	-	Thickness of the web

Greek notations and symbols

α_{F0}	-	Imperfection factor
γ_s	-	Relative flexural rigidity of the longitudinal stiffener
γ_{M1}	-	Partial factor for resistance of members to instability assessed by member checks
ε	-	Coefficient depending on the yield strength
η	-	Correction factor for the bending moment or imperfection factor
λ	-	Slenderness parameter
$\overline{\lambda_F}$	-	Equivalent compression flange slenderness
$\overline{\lambda_{F0}}$	-	Reference value for equivalent compression flange slenderness
ν	-	Poisson's ratio
φ_F	-	Value to determine the reduction factor for local buckling χ_F
χ_F	-	Reduction factor for local buckling
$\chi(\lambda)$	-	Resistance function

Abstract

Previous investigations proved that the patch loading resistance model of the EN1993-1-5 for longitudinally stiffened girders has a relatively large scatter and can lead to a significant underestimation of the patch loading resistance. In an attempt to improve the current situation, a large number of previous studies analysed the structural behaviour of longitudinally stiffened steel girders subjected to patch loading, but a simple and reliable design method is yet to be available in the international literature. The focus of the current paper is on the comparison of the design method of EN1993-1-5, design proposals of Davaine and Graciano et al., and a FEM analysis. The effect of several geometrical parameters on the patch loading resistance is reviewed for longitudinally stiffened steel girders with either an open or a closed section stiffener. Outer bounds of these parameters are also analysed for configurations with two or more stiffeners to check for similar effects as those seen in the case of a single longitudinal stiffener. In general, the design proposals of Davaine and Graciano et al. improve the design method as currently described in the EN1993-1-5. These methods, however, only take one stiffener into account while usually multiple stiffeners are applied on the web. The design proposals are in close correlation to FEM analyses for girders with one open section longitudinal stiffener. The patch loading resistance of girders with closed section stiffeners is underestimated.

Abstract in Dutch

Eerder onderzoek heeft aangetoond dat de weerstand van longitudinaal verstevigde stalen balken tegen veldgewijze belastingen (Engels: *patch loading*) volgens het model beschreven in EN1993-1-5, aanleiding geeft tot een relatief grote verspreiding van de resultaten en zelfs tot een onderschatting ervan. Een groot aantal onderzoeken analyseerden het structurele gedrag van deze longitudinaal verstevigde balken in een poging tot een simpele en betrouwbare ontwerpmethode voor de zogenoemde patch loading te creëren. De vergelijking van de ontwerpmethode en -voorstellen van zowel de EN1993-1-5, Davaine en Graciano et al. ten opzichte van een eindige elementenanalyse staat centraal in deze paper. De invloed van enkele geometrische parameters wordt nagegaan voor zowel verstevigingen met een open als gesloten sectie. Zo worden ook de uiterste parametergrenzen onderzocht voor configuraties met meerdere verstevigingen om een analoog gedrag terug te verifiëren. De ontwerpvoorstellen van zowel Davaine als die van Graciano et al. vormen een verbetering ten opzichte van de methode beschreven in EN1993-1-5. Echter ook deze voorstellen rekenen met slechts een enkele versteviging terwijl er in de praktijk veeleer configuraties met meerdere verstevigingen voorkomen. De ontwerpmethode en -voorstellen komen nauw overeen wanneer het over open sectie verstevigingen gaat, maar dit geldt niet zo voor de verstevigingen met een gesloten sectie; deze worden onderschat.

1 Introduction

Bridges can be constructed in various ways. For bridge decks greater than 250 meters in length, the method of incremental launching can be considered. With this method of construction, the bridge deck is built in sections by pushing the structure outwards from the abutments towards the pier. Figure 1 displays a schematic representation of this method.

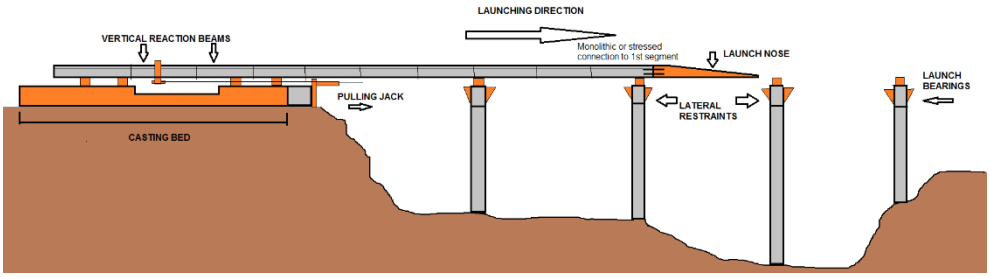

Figure 1: Schematic of the method of incremental launching [1].

During the incremental launching of bridges, patch loading is an important factor to consider. Patch loading happens when concentrated transverse loads are applied to one flange, over the loading length of a steel girder. To this date, the calculation of the patch loading resistance of longitudinally stiffened girders still lacks a reliable and simple design method [2]. The EN1993-1-5 describes the current design method, but it has a relatively large scatter. This can lead to a significant underestimation of the patch loading resistance of said girders. However, various new design methods have been proposed throughout the years and are available in the international literature [3].

1.1 Motivation

The major problem in the EN1993-1-5 is the lack of a reliable and simple design method to calculate the patch loading resistance of longitudinally stiffened girders. This is due to the shear complexity of the phenomenon. There are several variables that account for different resistances, e.g.: the number of longitudinal stiffeners attached to the web; the stiffness of the stiffeners; the placement of the stiffeners. These variables result in a different buckling behaviour of the girder web which in turn influences the patch loading resistance [2]. Figure 2 and Figure 3 display the possible buckling behaviours for a girder with only one longitudinal stiffener: (a) local buckling of the sub-panels, (b) interaction of the global and local buckling (coupled instabilities), and (c) global buckling of the web.

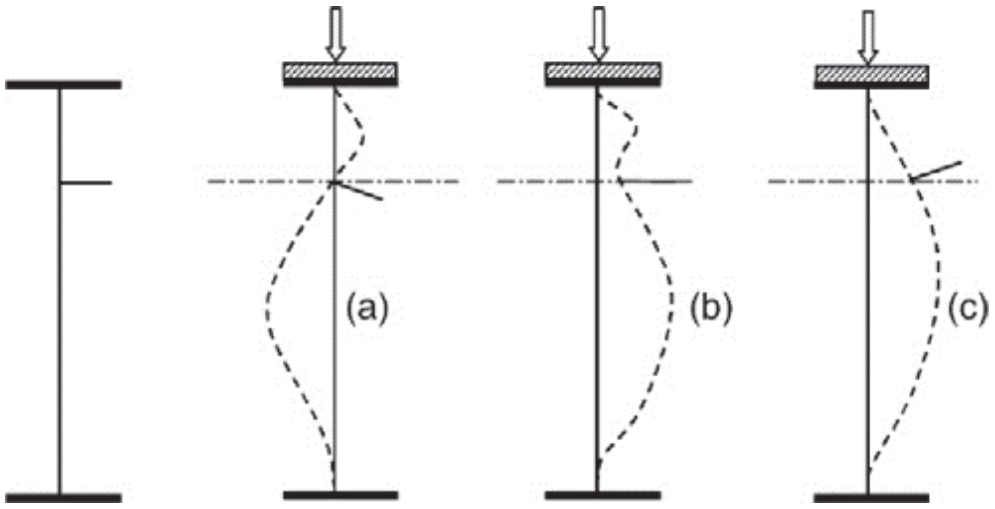

Figure 2: Failure mode types of girders with one longitudinal stiffener [2, p. 238].

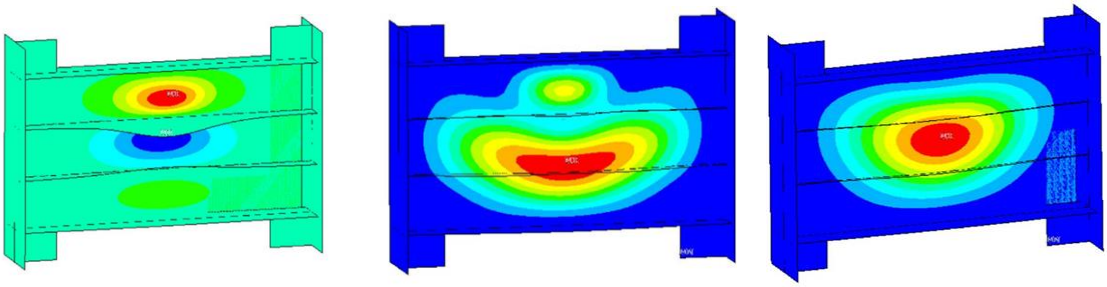

(a) (b) (c)

Figure 3: Typical web crippling failure modes [4, p. 196].

The main criticism of the current design method, as in EN1993-1-5, is that it has been developed for girders with only one longitudinal stiffener. Moreover, it covers the global, local, and coupled instabilities within one mechanical model [2]. This method is inapplicable for girders with more than one longitudinal stiffener. The second remark is that the location of the longitudinal stiffener is not considered properly. [5] proposed a design method to resolve this issue and the proposition does yield better results than the EN1993-1-5. However, this proposed design method is, once again, also developed for girders with only one stiffener, and, likewise, it underestimates the patch loading resistance [2]. The third point of criticism is the implementation of the longitudinal stiffener into the buckling coefficient k_f. This implies that an increase in the stiffener's stiffness results in an increase of the critical load amplifier and therefore in an increase of the patch loading resistance. However, if the stiffener is sufficiently rigid enough to separate the buckling shapes to the web's sub-panels (Figure 2.a and Figure 3.a), then a further increase of the stiffener's stiffness will not yield an amplification of the patch loading resistance [2].

1.2 Conventions

This thesis handles patch loading "type a" according to EN1993-1-5, depicted on Figure 4. Figure 5 displays the symbols for the various girder measurements for a girder stiffened with an open or a closed section stiffener.

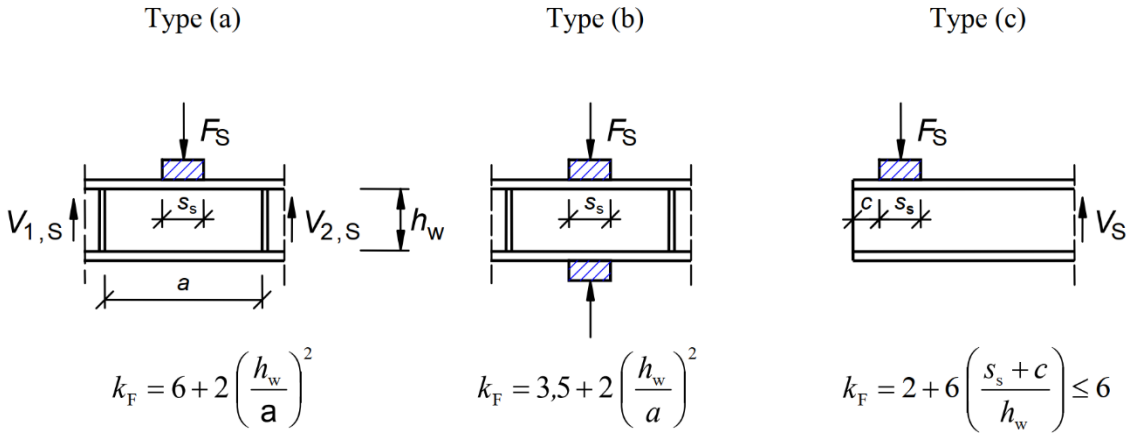

Figure 4: Buckling coefficients for different types of load application [6, p. 26].

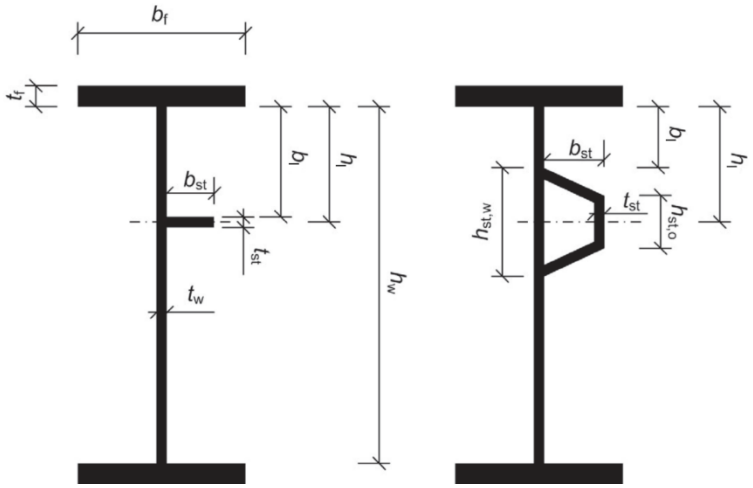

Figure 5: Schematic description for cross-sectional notations for a girder stiffened with an open section stiffener (left) and a closed section stiffener (right) [7, p. 26].

The hitherto known design methods using reduction factors require the calculation of the moment of inertia of the longitudinal stiffener closest to the loaded flange ($I_{sl,1}$). According to EN1993-1-5, the effective cross-section (Figure 6) is to be considered.

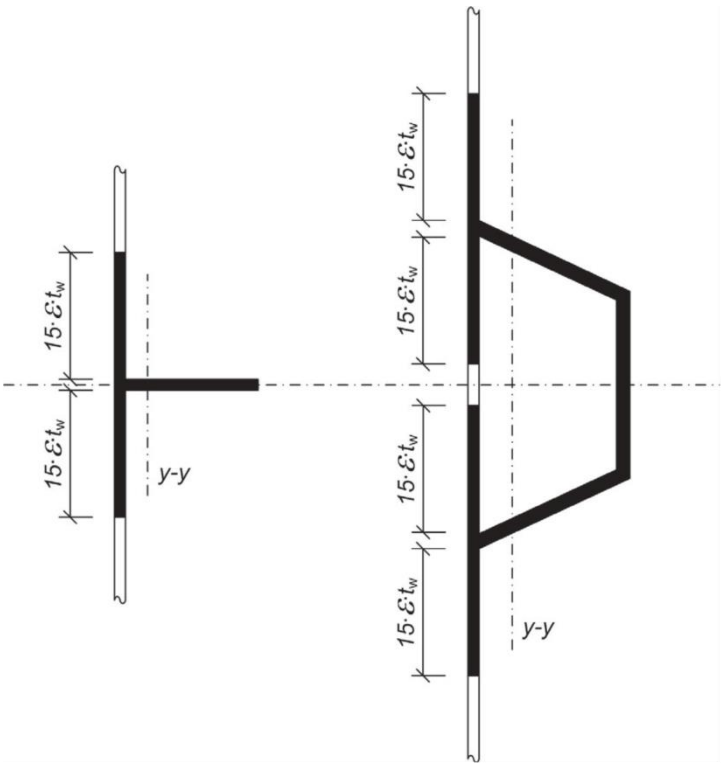

Figure 6: The effective cross-section of an open section longitudinal stiffener (left) and a closed section longitudinal stiffener (right), according to EN1993-1-5 [7, p. 26].

1.3 Objectives and delimitation

The aim of the current research is to describe and evaluate the most important known design methods and proposals. This evaluation includes a comparison of the design methods and proposals to FEM analyses of the exact same girders. A parameter study reveals the influence of the different girder measurements. The girder models are based on those of Seitz [8] and Kövesdi [2], [4].

1.4 Overview

The first segment on the topic of the calculations of patch loading resistance includes a literature review that describes the most important design methods and proposals. This segment is split up in methods that use magnification factors and those that use reduction factors. Following the literature review there is a segment that describes the methods and actions for the calculations, as well as various material properties of the girders. Results and discussion describe the findings and compares and explains the gathered data. Lastly, Summary and conclusions closes the research work by briefly summarising the findings.

2 Literature review

The determination of the patch loading resistance of longitudinally stiffened girders still has room for improvement: despite numerous previous investigations, [9] found even the best currently-known design recommendation can result in a 20-60% underestimation of the patch loading resistance when compared to experimental test results [2]. The resistance increasing effect of the longitudinal stiffeners can be determined by two general design principles. The first principle uses magnification factors, while the second uses reduction factors. Calculation proposals for the former will be discussed in 2.1, and those for the latter in 2.2.

2.1 Design methods using magnification factors

The strategy that all design methods using magnification factors have in common is to multiply the calculated patch loading resistance for an unstiffened girder with an amplification factor $f(s)$, in order to estimate the actual resistance of the longitudinally stiffened girder, i.e., Equation (1).

$$F_{Rl} = F_R \cdot f(s) \tag{1}$$

Where F_{Rl} and F_R are the patch loading resistances of the longitudinally stiffened girder and unstiffened girder, respectively. Various important proposals for the amplification factor $f(s)$ and for the patch loading resistance of unstiffened girders F_R will be discussed in the following subsections.

2.1.1 Bergfelt

In 1997, [10] presented a three-hinge-flange model together with a resistance function for unstiffened girders. Bergfelt's investigations were initially meant as an attempt to improve the calculation method for unstiffened girders, but Bergfelt proposed Equation (2) as the amplification factor for a longitudinally stiffened girder after comparison with the (relatively few and scattered) test results [7].

$$f(s) = 1 + \left(\frac{1}{3} + \frac{b_l}{h_w}\right) \cdot \sqrt{\frac{s_\eta}{3 \cdot b_l}};\ 0.1 < \frac{b_l}{h_w} < 0.33 \tag{2}$$

in which the modified distance between the outermost plastic hinges in the loaded flange is proposed to lie in the interval

$$s_y + s_s \leq s_\eta \leq s_y + s_s + \frac{{s_s}^2}{s_y} \tag{3}$$

Bergfelt proposes Equation (4) to determine the distance between the outermost plastic hinges.

$$s_y = 5.2 \cdot \frac{b_f}{\eta} \cdot \left(\frac{t_f}{t_w}\right)^2 \cdot \sqrt{\frac{t_w}{t_i}} \cdot \frac{f_{yf}}{\sqrt{E \cdot f_{yw}}} \tag{4}$$

where the correction factor for the flange bending, η, is read from Table 1 and the idealised flange thickness t_i can be acquired using Equation 5.

Table 1: η-factor in Bergfelt's formula [11, p. 15].

t_f/t_w	0	2	3	4	5	6
η	1	1	1.14	1.35	1.405	1.405

$$\begin{cases} t_i = t_f & if\ \frac{b_f}{t_f} = 25 \\ t_i = t_f \cdot \sqrt[4]{\frac{b_f}{25 \cdot t_f}} & if\ \frac{b_f}{t_f} \neq 25 \end{cases} \tag{5}$$

Equations 6 and 7 are to be used respectively to calculate the estimated patch loading resistance of an unstiffened girder, and the needed correction factor for the loaded length.

$$F_R = 0.8 \cdot {t_w}^2 \cdot \sqrt{E \cdot f_{yw}} \cdot \sqrt{\frac{t_i}{t_w}} \cdot f(s_s) \tag{6}$$

$$f(s_s) = 1 + 40 \cdot \frac{s_s}{s_\eta} \cdot \frac{t_w}{h_w} \tag{7}$$

2.1.2 Marković and Hajdin

In 1992, [12] suggested Equation (8), a linear equation, as recommendation for an amplification factor, derived based on test data from the reviewed literature. This database consists of 133 longitudinally stiffened and 318 unstiffened girders [7].

$$f(s) = 1.28 - 0.7 \cdot \frac{b_l}{h_w}; 0.1 < \frac{b_l}{h_w} < 0.4 \tag{8}$$

Roberts proposed to determine F_R via Equation (9), in 1981.

$$F_R = 0.5 \cdot {t_w}^2 \cdot \sqrt{\frac{E \cdot f_{yw} \cdot t_f}{t_w}} \cdot \left[1 + \frac{3 \cdot s_s}{h_w} \cdot \left(\frac{t_w}{t_f}\right)^{\frac{3}{2}}\right] \tag{9}$$

This equation assumes f_{yf} and f_{wf} to be equal. Due to the somewhat unrealistic assumption of the presence of a straight flange between the two inner plastic hinges for an increasing loaded length, Roberts recommended to limit the ratio s_s/h_w to 0.2 [7]. Furthermore, [12]

concluded Roberts' proposal the hitherto best formula to predict the resistance of the unstiffened girders, given a diminished influence of the loading length.

2.1.3 Kutmanová and Skaloud

Based on an empirical formulation for the unstiffened web, [13] proposed a magnification factor (Equation 10) for the consideration of the longitudinal stiffener in 1988, and improved the formulation in 1992. The calculation of the estimated patch loading resistance of unstiffened girders follows Equation 11.

$$f(s) = 0.958 - 0.09 \cdot \ln\left(\frac{b_l}{h_w}\right) \tag{10}$$

$$F_R = 12.6 \cdot {t_w}^2 \cdot f_{yw} \cdot \left(1 + 0.004 \cdot \frac{s_s}{t_w}\right) \cdot \left(\frac{I_f}{{t_w}^4} \cdot \sqrt{\frac{f_{yf}}{240}}\right)^{0.153} \tag{11}$$

2.1.4 Graciano

In 2002, [11] studied the patch loading resistance of longitudinally stiffened steel girders and found Equations 12 and 20 to, respectively, describe the estimated patch loading resistance of an unstiffened girder, and the magnification factor.

$$F_R = F_y \cdot \chi(\lambda) \tag{12}$$

Where the yield resistance F_y and the effective loaded length l_y should be calculated by

$$F_y = f_{yw} \cdot t_w \cdot l_y \tag{13}$$

$$\begin{cases} l_y = s_s + 2 \cdot t_f \cdot (1 + \sqrt{m_1 + m_2}) & if\ l_y \le a \\ l_y = a & if\ l_y > a \end{cases} \tag{14}$$

m_1 and m_2 are dimensionless parameters

$$m_1 = \frac{f_{yf} \cdot b_f}{f_{yw} \cdot t_w} \qquad \text{and} \qquad m_2 = 0.02 \cdot \left(\frac{h_w}{t_f}\right)^2 \tag{15}$$

for welded girders m_2 should be taken as zero if $\lambda < 0.5$.

The resistance function $\chi(\lambda)$ is

$$\chi(\lambda) = 0.06 + \frac{0.47}{\lambda} \le 1.0 \tag{16}$$

where λ equals the slenderness parameter with the critical buckling load F_{cr} calculated as given in Equation 18.

$$\lambda = \sqrt{\frac{F_y}{F_{cr}}} \tag{17}$$

$$F_{cr} = k_F \cdot \frac{\pi^2 \cdot E \cdot {t_w}^3}{12 \cdot (1-\nu^2) \cdot h_w} \tag{18}$$

The buckling coefficient k_F is given by

$$k_F = 5.82 + 2.1 \cdot \left(\frac{h_w}{a}\right)^2 + 0.46 \cdot \sqrt[4]{\frac{b_f \cdot {t_f}^3}{h_w \cdot {t_w}^3}} \tag{19}$$

[11] found that not only the location of the stiffener $\left({}^{b_l}/_{h_w}\right)$, but also the ratio of flange to web thickness $\left({}^{t_f}/_{t_w}\right)$ and the ratio of the yield strength of the flange to the yield strength of the web $\left({}^{f_{yf}}/_{f_{yw}}\right)$ influences the resistance of the longitudinally stiffened girder. Hence the inclusion of these parameters in Equation 20.

$$f(s) = 0.556 - 0.277 \cdot \ln\left[\frac{b_l}{h_w} \cdot \left(\frac{f_{yf}}{f_{yw}} \cdot \frac{t_w}{t_f}\right)\right]; 0.1 \leq \frac{b_l}{h_w} \leq 0.3 \tag{20}$$

2.2 Design methods using reduction factors

The design methods using reduction factors form the second group of design methods. The reduction factor χ_F should be evaluated by the same equation for both longitudinally stiffened and unstiffened girders. The effect of the longitudinal stiffeners is implemented in the buckling coefficient k_F and the critical load F_{cr}. The current design method, described in the EN1993-1-5, is a reduction factor-based design method developed by Graciano, Lagerqvist and Johannson [2], and will be discussed in 2.2.1.

2.2.1 Graciano, Lagerqvist and Johannson

Graciano's 2002 investigations form the basis of the in 2005 developed design method. This model is based on Graciano's Model III [11] and allows the calculation of the patch loading resistance by utilising Equation 21.

$$F_{Rd} = \frac{\chi_F \cdot l_y \cdot f_{yw} \cdot t_w}{\gamma_{M1}} \tag{21}$$

The reduction factor due to local buckling χ_F should be acquired by Equations 22 through 25.

$$\chi_F = \frac{1.0}{\varphi_F + \sqrt{{\varphi_F}^2 - \overline{\lambda_F}}} \leq 1.0 \tag{22}$$

where

$$\varphi_F = \frac{1}{2} \cdot \left[1 + \alpha_{F0} \cdot \left(\overline{\lambda_F} - \overline{\lambda_{F0}}\right) + \overline{\lambda_F}\right] \tag{23}$$

$$\overline{\lambda_F} = \sqrt{\frac{l_y \cdot t_w \cdot f_{yw}}{F_{cr}}} \tag{24}$$

and where the following values should be used in case of bridges ($\gamma_{M1} = 1.10$):

$$\alpha_{F0} = 0.75 \qquad \text{and} \qquad \overline{\lambda_{F0}} = 0.50 \qquad \text{if} \qquad \gamma_{M1} = 1.10 \tag{25}$$

The effective loaded length can be calculated by

$$\begin{cases} l_y = s_s + 2 \cdot t_f \cdot (1 + \sqrt{m_1 + m_2}) & if\ l_y \leq a \\ l_y = a & if\ l_y > a \end{cases} \tag{14}$$

where m_1 and m_2 are dimensionless parameters. m_2, however, equals zero here because $\overline{\lambda_{F0}} \geq 0.50$.

$$m_1 = \frac{f_{yf} \cdot b_f}{f_{yw} \cdot t_w} \qquad \text{and} \qquad m_2 = 0.02 \cdot \left(\frac{h_w}{t_f}\right)^2 = 0 \tag{15}$$

In order to calculate the critical buckling load F_{cr}, the buckling coefficient k_F is to be obtained from Equation 26 for unstiffened girders, or Equations 27 and 28 for longitudinally stiffened girders.

$$F_{cr} = k_F \cdot \frac{\pi^2 \cdot E \cdot {t_w}^3}{12 \cdot (1 - \nu^2) \cdot h_w} \tag{18}$$

$$k_F = 6 + 2 \cdot \left(\frac{h_w}{a}\right)^2 \tag{26}$$

$$k_F = 6 + 2 \cdot \left(\frac{h_w}{a}\right)^2 + \left(5.44 \cdot \frac{b_l}{a} - 0.21\right) \cdot \sqrt{\gamma_s} \tag{27}$$

$$\gamma_s = 10.9 \cdot \frac{I_{sl,1}}{h_w \cdot {t_w}^3} \leq 13 \cdot \left(\frac{a}{h_w}\right)^3 + 210 \cdot \left(0.3 - \frac{b_l}{a}\right) \tag{28}$$

In Equation 28, $I_{sl,1}$ is the second moment of area of the stiffener closest to the loaded flange, including contributing parts, such as an effective plate width of $15 \cdot \varepsilon \cdot t_w$ on both sides of the stiffener [6]. Where ε is defined as

$$\varepsilon = \sqrt{\frac{235}{f_{yw}}} \tag{29}$$

However, this design method is mainly developed for girders with merely a single longitudinal stiffener that is placed withing the range of Equation 30, close to the loaded flange.

$$0.05 \leq \frac{b_l}{a} \leq 0.3 \qquad \text{and} \qquad \frac{b_l}{h_w} \leq 0.3 \tag{30}$$

2.2.2 Davaine

Complementing the EN1993-1-5, Davaine's 2004 and 2005 studies focused not only on the elastic critical load, but also included a complete reduction factor approach [5], [7]. Davaine's work concerning the elastic critical load aimed for taking the buckling of the upper panel into account for the expression used to estimate the elastic critical load of the web. By performing a regression analysis on the results of 366 numerical FE simulations, an expression for the buckling coefficient concerning the upper panel was derived:

$$k_{F,2} = \left(0.8 \cdot \frac{s_s+2\cdot t_f}{a} + 0.6\right) \cdot \left(\frac{a}{b_l}\right)^{\left(0.6\cdot\frac{s_s+2\cdot t_f}{a}+0.5\right)} \tag{31}$$

$$F_{cr,2} = k_{F,2} \cdot \frac{\pi^2 \cdot E \cdot {t_w}^3}{12\cdot(1-\nu^2)\cdot b_l} \tag{32}$$

While Graciano's buckling coefficient describes the panel as a whole, Equations 31 and 32 predict the elastic critical load of the upper panel alone. These formulae would only be valid if the following expression is true:

$$s_s + 2 \cdot t_f + 2 \cdot b_l \leq a \tag{33}$$

Davaine also proposed an interaction formula for the two buckling modes:

$$F_{cr} = \frac{F_{cr,1}\cdot F_{cr,2}}{F_{cr,1}+F_{cr,2}} \tag{34}$$

$F_{cr,1}$ can be obtained via Equation 18 using the buckling coefficient according to Equation 27. However, Davaine's proposal for the improved reduction factor function states modified values for α_{F0} and $\overline{\lambda_{F0}}$ in Equation 23:

$$\alpha_{F0} = 0.21 \qquad \text{and} \qquad \overline{\lambda_{F0}} = 0.80 \tag{35}$$

Furthermore, Davaine also proposed to set the term $m_2 = 0$ regarding Equation 14.

2.2.3 Graciano, Lagerqvist and Mendes

Complementing the EN1993-1-5, [14] aimed to improve the expression for the buckling coefficient for longitudinally stiffened beams subjected to patch loading. A linear buckling analysis using FEM was performed at first. To weigh the geometrical parameters on the buckling coefficient, a first order factorial design was conducted, followed by a second order model to predict the buckling coefficient of longitudinally stiffened plate girders. In this 2014 study, Graciano and Mendes investigated 882 numerical models.

Equation 36 represents the second-order equation. However, for practical purposes, this equation is limited and difficult to use. Therefore, [14] performed a regression analysis using the least square method in order to obtain an expression for the contribution of longitudinal stiffening, using real variables, such as: b_l/h_w, s_s/a, γ_s and t_f/t_w. This expression is given by Equation 37 and is to be utilised in Equation 38 in order to calculate the buckling coefficient.

$$k_F = 14.98 + 3.51 \cdot x_1 - 0.55 \cdot {x_1}^2 + 1.57 \cdot x_2 + 0.31 \cdot {x_2}^2 + 1.72 \cdot x_3 + 0.36 \cdot x_4 + 0.63 \cdot x_1 \cdot x_2 + 1.12 \cdot x_1 \cdot x_3 + 0.28 \cdot x_2 \cdot x_3 \quad (36)$$

$$k_{sl} = -1.87 + 36.94 \cdot \frac{b_l}{h_w} - 62.86 \cdot \left(\frac{b_l}{h_w}\right)^2 - 8.09 \cdot \frac{s_s}{a} + 16.38 \cdot \left(\frac{s_s}{a}\right)^2 - 0.0036 \cdot \gamma_s + 0.44 \cdot \frac{t_f}{t_w} + 30.95 \cdot \frac{b_l}{h_w} \cdot \frac{s_s}{a} + 0.031 \cdot \frac{b_l}{h_w} \cdot \gamma_s + 0.0035 \cdot \frac{s_s}{a} \cdot \gamma_s \quad (37)$$

$$k_F = 6 + 2 \cdot \left(\frac{h_w}{a}\right)^2 + k_{sl} \quad (38)$$

3 Method and materials

In this section, the method of calculation and general material properties are discussed. The different approaches to the calculations are elaborated on in their own distinct subchapter. The functions used to calculate the maximum patch loading according to the design methods and proposals are discussed in the second subchapter. This is followed by the development of the numerical model and the verification of it.

3.1 Applied material models

For every panel, the steel grade S355 is applied. This steel grade has a yield strength (f_y) equal to 355 MPa and an ultimate strength (f_u) of 510 MPa. The material is assumed to behave elastoplastic: it has a linearly elastic and a perfectly plastic section. The Young's modulus equals to 210000 MPa up to the yield stress.

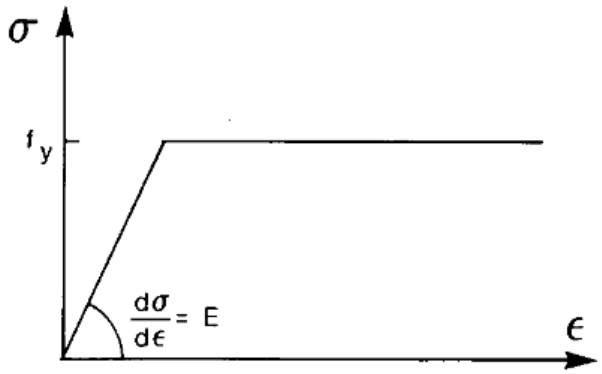

Figure 7: Bi-linear stress-strain relationship [6, p. 39].

3.2 Models

The basic model regarding open section stiffeners is based on Kövesdi's *Specimen #3* [4]. Likewise, the basic model with closed section stiffeners is based on Seitz' *Versuchsträger IV* [8]. Basic model dimensions are included in Table 2. The naming scheme is as follows: *researcher of the original model – number of stiffeners – changed parameter*. The parametric range for these each of these base models is pictured in Table 3. The full investigation was done for the models with only one stiffener. For models with two or three stiffeners, only the outer values of the given parametric range were investigated to ascertain the influence of the parameter, and b_l was not studied. Figure 8 until Figure 12 display the basic models with both open and closed section stiffeners, while Figure 13 displays a detailed view of a closed section stiffener. A complete list of the analysed models, including parameters, is included in Appendix A.

Table 2: Basic model dimensions; dimensions given in mm, yield strengths in N/mm².

Specimen	t_w	a	h_w	f_{yw}	t_f	b_f	f_{yf}	s_s	b_l	t_{st}	$h_{st,o}$	$h_{st,w}$	b_{st}
Kövesdi-1	4	1000	500	355	10	150	355	200	123	4	0	0	40
Kövesdi-2	4	1000	500	355	10	150	355	200	123	4	0	0	40
Kövesdi-3	4	1000	500	355	10	150	355	200	123	4	0	0	40
Seitz-1	6	2400	1200	355	20	260	355	700	250	4	50	100	100
Seitz-2	6	2400	1200	355	20	260	355	700	250	4	50	100	100

Table 3: Parametric table for Kövesdi-based models (left), and Seitz-based models (right).

Parameter	Min.	Max.	Increment
t_w	3	8	1
s_s	50	350	50
b_l	50	150	25
t_{st}	3	8	1
b_{st}	25	75	10

Parameter	Min.	Max.	Increment
t_w	3	8	1
s_s	100	1200	100
b_l	120	320	40
t_{st}	3	8	1
$h_{st,o}$	20	80	10
$h_{st,w}$	50	200	25
b_{st}	50	150	10

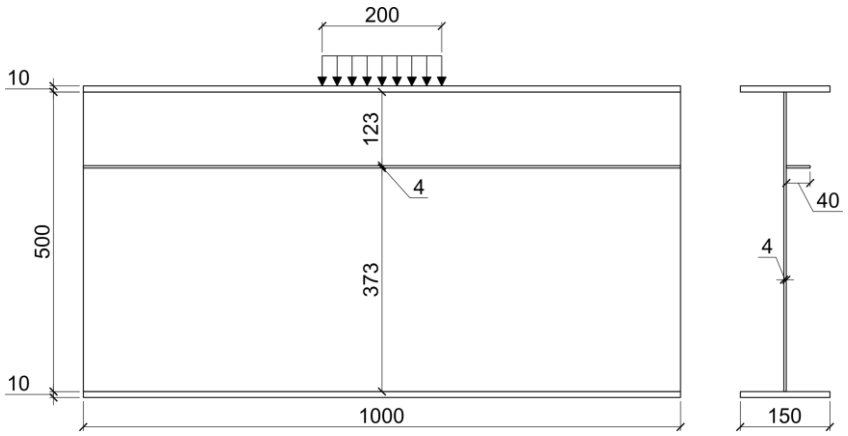

Figure 8: Standard configuration of Kövesdi-1.

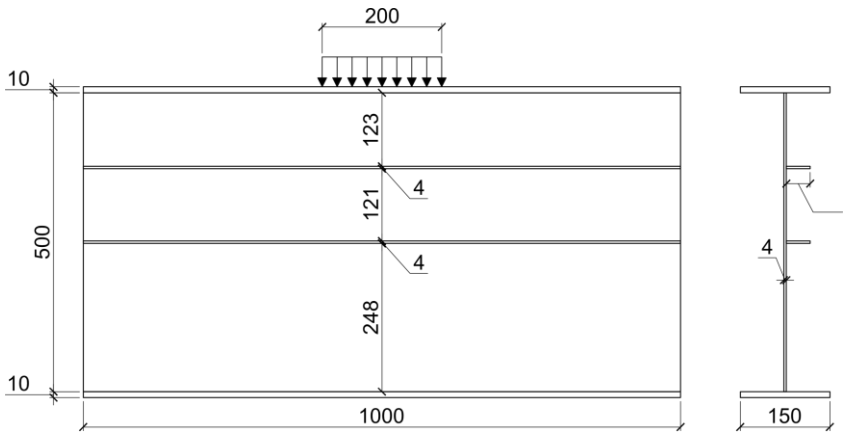

Figure 9: Standard configuration of Kövesdi-2.

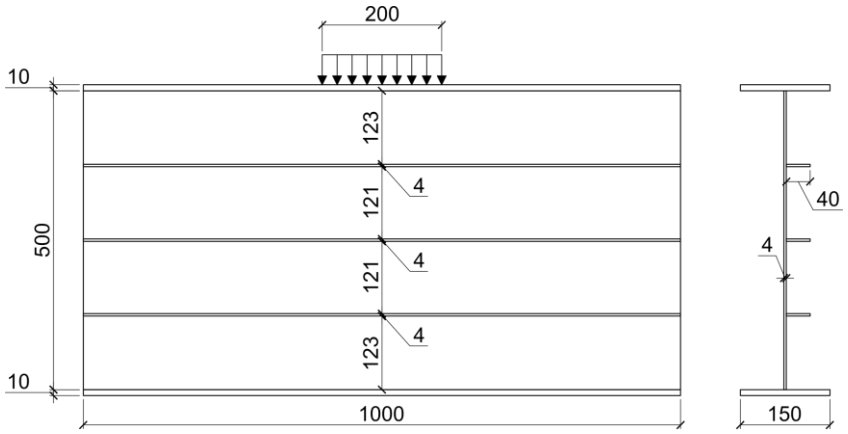

Figure 10: Standard configuration of Kövesdi-3.

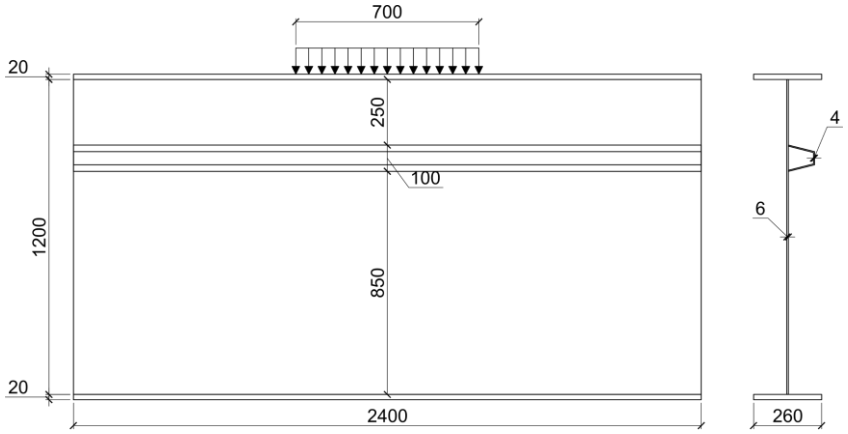

Figure 11: Standard configuration of Seitz-1.

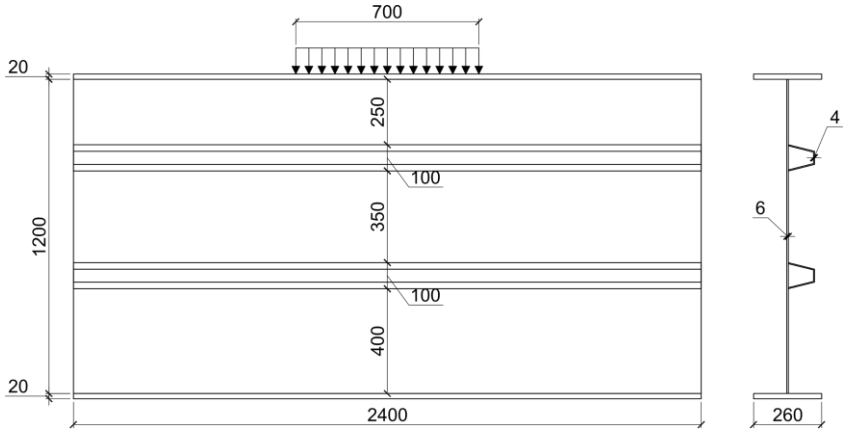

Figure 12: Standard configuration of Seitz-2.

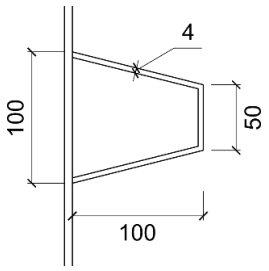

Figure 13: Standard stiffener configuration of Seitz' models.

3.3 Design methods

Because of the dated calculation approach of the design methods using magnification factors – described in 2.1 – only the design methods using reduction factors – described in 2.2 – are calculated. These calculations were performed using script files programmed in MATLAB R2020a. In short, the scripts read the necessary data from a datasheet on a row per row basis, perform the calculations for each design method, and write the results in the exact same datasheet. Appendix B includes code to calculate the patch loading resistance for both longitudinally stiffened and unstiffened steel girders. A brief overview of the items is given in Table 4.

Table 4: Overview of the included code.

File name	**Description**
RunCalculations.m	Runs the calculations form the given dataset.
calcIsl1.m	Calculates the second moment of area of a stiffener.
GLJ_Unstiffened.m	Patch loading resistance calculation according to EN1993-1-5; developed by Graciano, Lagerqvist and Johansson; for unstiffened girders. (Not used in the current research.)
GLJ.m	Patch loading resistance calculation according to EN1993-1-5; developed by Graciano, Lagerqvist and Johansson; for longitudinally stiffened girders.
Davaine.m	Patch loading resistance calculation according to Davaine; for longitudinally stiffened girders.
GLM.m	Patch loading resistance calculation according to Graciano, Lagerqvist and Mendes; for longitudinally stiffened girders.

3.4 Numerical model development and verification

3.4.1 Geometrical model and applied analysis method

The numerical calculations are preformed using CIMNE's GiD 14.0.2 and GREISCH's FINELG 10.0 [15]. The numerical modelling is based on a full shell model using four-node thin shell elements. Figure 14 depicts the finite element model (or FEM) mesh of developed models, where the loading length s_s is represented by the downward facing arrows on top of the models, and the support conditions are shown by the lines at the outer sides of the models. The support conditions are assumed to be perfectly fixed along the hereby indicated outer sides of the models.

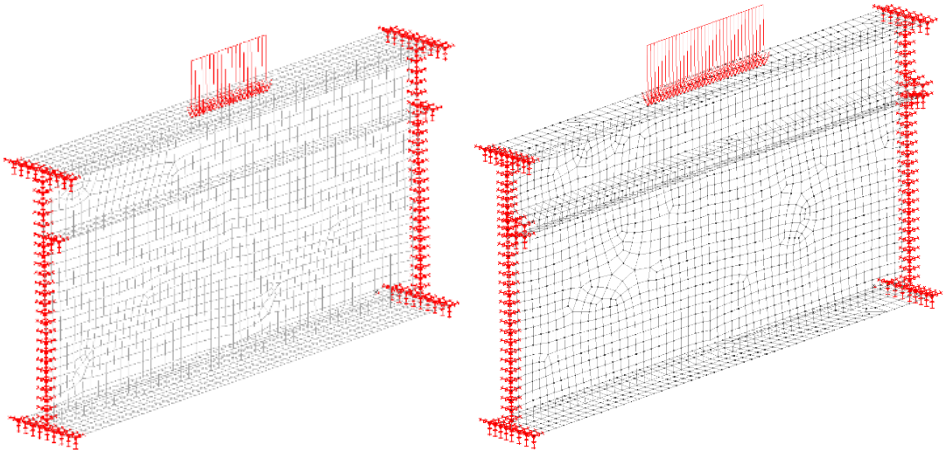

Figure 14: Finite element mesh of the models with an open section stiffener (left) and a closed section stiffener (right).

A remark about this software is that problems may arise when moving nodes that are part of a surface with already defined properties, using the included FINELG tools. This may leave the "surface properties" floating in the original space and results in a warped mesh generation. Figure 15 displays this behaviour.

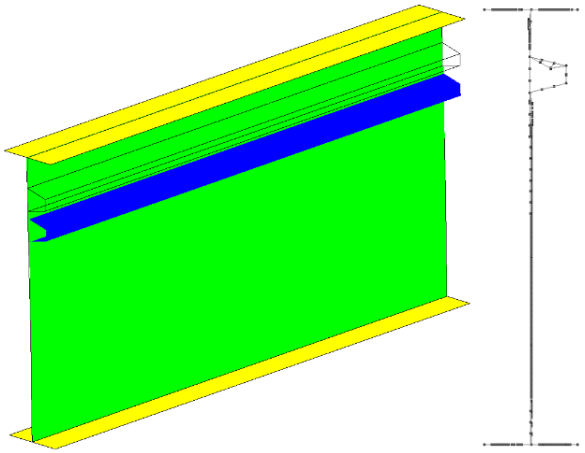

Figure 15: Surface properties view (left), and generated mesh view (right).

The patch loading resistance is determined by a nonlinear analysis using equivalent geometric imperfections (or GMNI). In the force-driven nonlinear analysis, the Newton-Raphson approach is used. More specifically, FINELG's type 4: *Pas de Newton-Raphson + FHE + SAUT*. This method is identical to the Newton-Raphson approach with the exception that it applies $dP + FHE$ instead of only dP, and that if the previous step has converged, the first iteration of the new step is skipped. If it did not converge, $dP + FHE$ is used. The exact parameters are depicted in Appendix C.

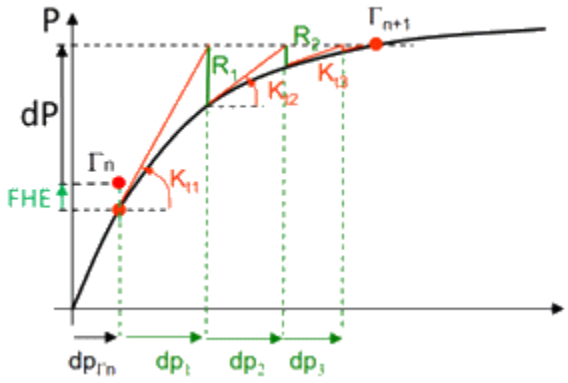

Figure 16: Pas de Newton-Raphson + FHE + SAUT [15].

To determine an appropriate finite element mesh size, a mesh convergence study is executed for both basic models. Displayed in Figure 17 are the results of the convergence study for Kövesdi-based models. A mesh size ranging from 10 to 40 mm with intervals of 5 mm, was tested. Although the patch loading resistance seems to increase when increasing the average mesh size (depicted as a blue line and markers), this is not the case as this phenomenon is due to inaccuracies. The smaller the average mesh size is, the higher the required amount of elements is to cover the complete model (depicted as grey columns) and thus the more complex the calculations become and the more time is needed to calculate the results. The

selected average mesh size is 15 mm. The patch loading resistance in case of an average mesh size of 10 or 15 mm is roughly equal, however, more than double the number of finite elements is needed for the average mesh size of 10 mm. For Seitz-based models, Figure 18 displays a similar curve. The average mesh size of 40 mm, however, gives a decreased patch loading resistance when compared the result of 35 mm. This is due to the guessing nature of the iterating calculation. The selected average mesh size is 30 mm for these models.

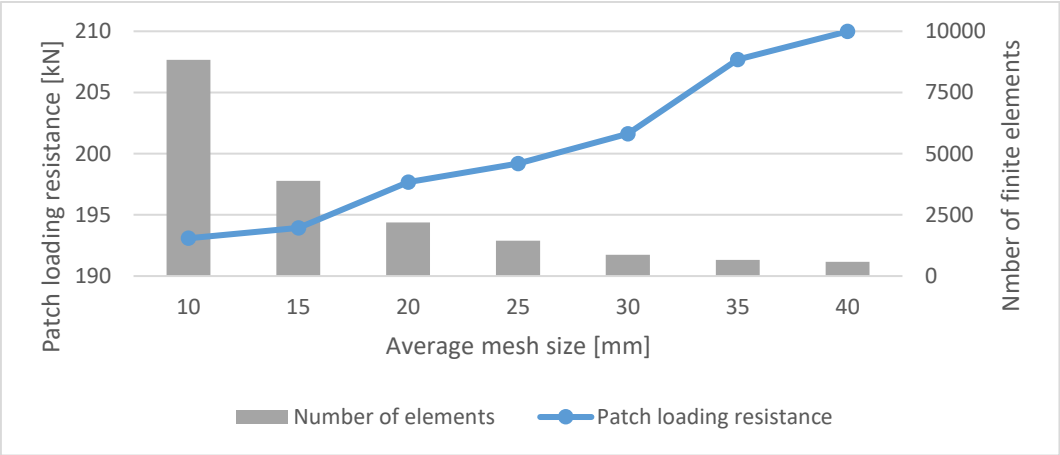

Figure 17: Results of the mesh convergence study for Kövesdi-based models.

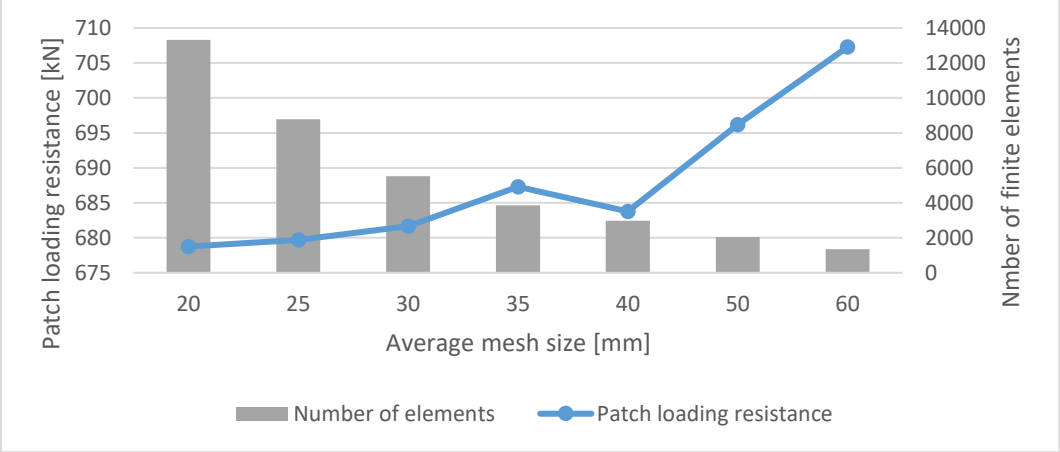

Figure 18: Results of the convergence study for Seitz-based models.

3.4.2 Applied imperfections

The applied imperfections consist of global and local imperfections. The global imperfections equal $h_w/400$ and are applied on the web at the height of the stiffeners and will thus move the stiffeners. The local imperfections are equal to $h_{w,i}/200$ and are placed at midheight of the subpanel. Both the global and local imperfections are applied using their full amplitude, overestimating the initial imperfection and deformation, but resulting in a safe patch loading resistance. [2] found that the applied imperfection shape results in a decrease in patch loading resistance of around 10%, and the ratio of the numerical and experimental resistances vary between 88 and 99%. Furthermore, the worst case for single-stiffener configurations is a negative global imperfection and negative local imperfection on the upper subpanel, combined with a positive imperfection on the lower subpanel. This imperfection shape is presented by *case 5* in Figure 19.

In all models, the stiffeners are placed with a negative global imperfection. For two or less stiffeners, only the lower subpanel has positive local imperfections, while for three stiffeners, the local imperfections are alternated with the lower subpanel always being placed with a positive imperfection.

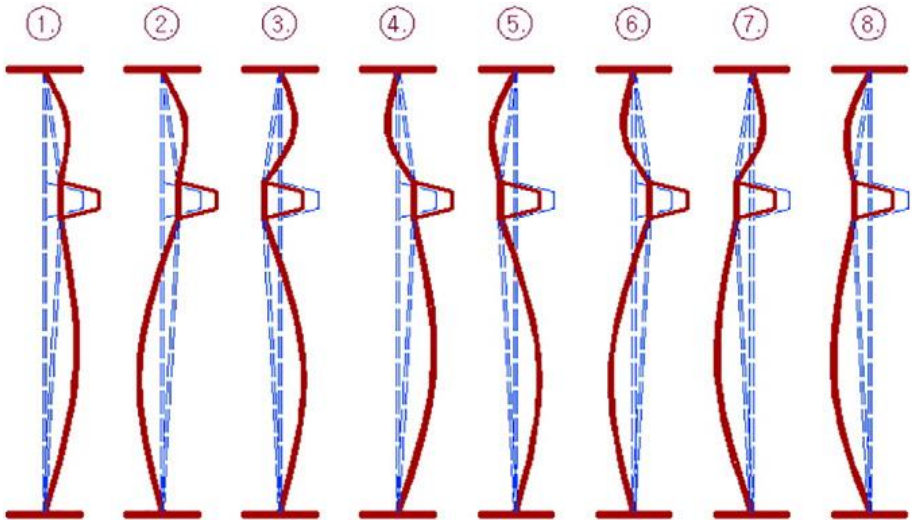

Figure 19: Applied imperfections in the sensitivity analysis [2].

The first step of the application of the imperfections, is to determine the global imperfection and move the stiffeners accordingly. Then NURBS (non-uniform rational B-spline) lines are drawn from flange to stiffener, and if needed from stiffener to stiffener. These are then divided at midheight of the subpanel. The location of this node at midheight can then be adjusted to reflect the respective local imperfections. In case of close section stiffeners, the section of the web panel at the stiffener itself should be a straight line.

3.4.3 Model verification

The validation procedure contains a comparison of the calculated resistances and existing results. Table 5 displays the patch loading resistances for all standard configurations of both basic models. As mentioned earlier, the models researched in this project are not exact replicas of the already existing models but are based on them. This means that the patch loading resistances will differ, although the general magnitude remains a valid source to validate the models. For Kövesdi-1, *Specimens #1* and #2 form comparable data that was found in [4]. Since Kövesdi-1 has only one stiffener, the predicted result should lie somewhere between *Specimen #1* that has no stiffener at all and *Specimen #2* that has two stiffeners. *Specimen #2* is used as point of reference for Kövesdi-2, although the stiffener spacing differs. In case of three open-section stiffeners, Kövesdi-3 can be compared to *Specimen #3*. The Seitz-based models can be compared to data found in Seitz' original work [8] and Kövesdi's further testing of configurations with one stiffener [2].

Table 5: Comparison of the patch loading resistances for the numerical model verification.

Specimen	$F_{Seitz,\ exp}$	$F_{Seitz,\ num}$	$F_{Kövesdi,\ exp}$	$F_{Kövesdi,\ num}$	$F_{R,\ num}$
Kövesdi-1			206 - 258	205 - 255	194
Kövesdi-2			258	255	212
Kövesdi-3			271	267	207
Seitz-1	1024	1023	1034	1030	683
Seitz-2	1219	1181			1121

The in this project numerically calculated patch loading resistances are significantly lower than those found in other research papers. This is due to various changes in the models and due to the use of large imperfections because they are dependent on the shape and magnitude of the applied imperfections [4]. As previously mentioned, and now proven by the results of the comparison, the usage of the complete amplitudes for both the local and global imperfections lead to patch loading resistances on the conservative side. Optimisation of the applied imperfections are available through the application of e.g.: the first eigenmode shape, a hand defined sinusoidal local or global imperfection shape, or a combination of local and global imperfection shapes where the defining imperfection shape if fully accounted for while the other shape's amplitude is reduced to about 70% [4].

4 Results and discussion

This section describes and discusses the observed failure modes, and the results acquired from the calculations according to the design methods and proposals, and this in comparison to the FEM analyses. The models with open section stiffeners – or Kövesdi-based models – and those with closed section stiffeners – or Seitz-based models – are discussed separately. Both of these subsections are further divided into the effect of a single variable parameter. Appendix D includes the calculated results.

4.1 Observed failure modes

The structural behaviour can be classified into three categories: local buckling of the subpanels, global buckling of the web, and interactive buckling (a combination of the two). Figure 20 until Figure 22 display the local buckling of the subpanels. Figure 20 and Figure 22 display the failure of the upper and lower subpanel respectively, while Figure 21 shows a somewhat even failure. Interactive failure is represented by Figure 23, and the global web buckling by Figure 24. The complete figures with corresponding legends are available in Appendix E, along with load-displacement diagrams.

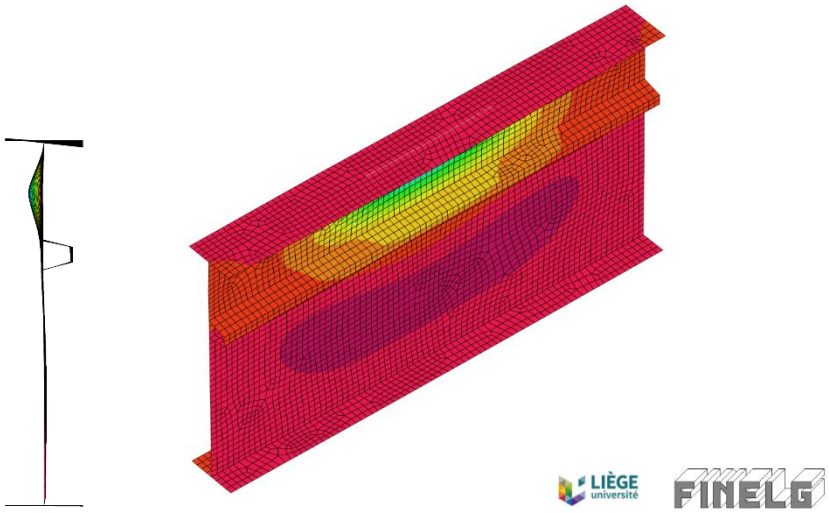

Figure 20: Local buckling; failure of the upper subpanel; Seitz-1-bl320 [15].

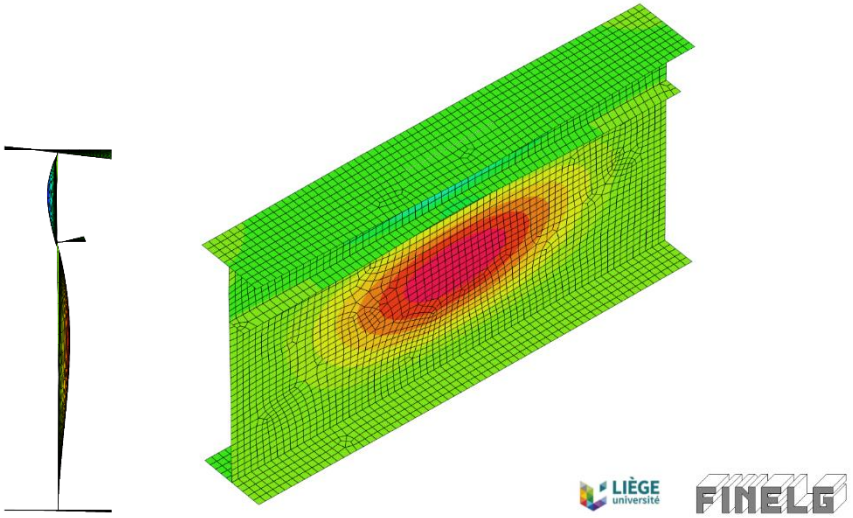

Figure 21: Local buckling; about even failure; Kövesdi-1 [15].

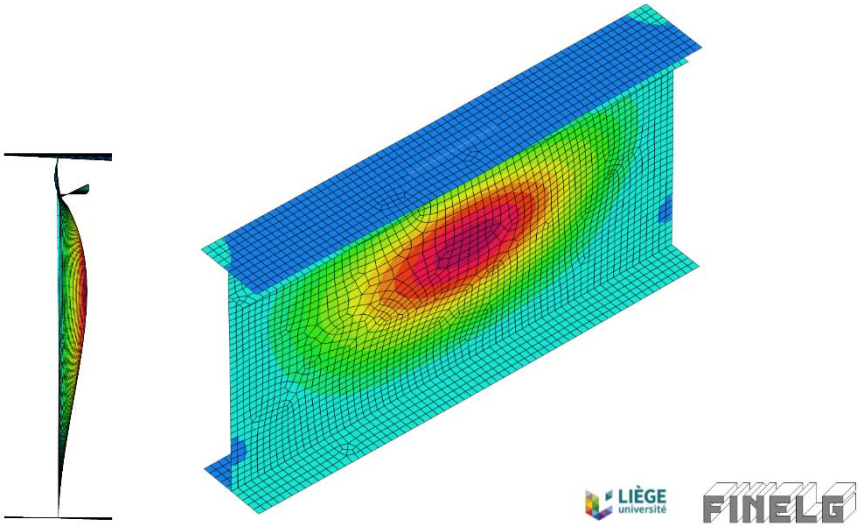

Figure 22: Local buckling; failure of the lower subpanel; Kövesdi-1-bl50 [15].

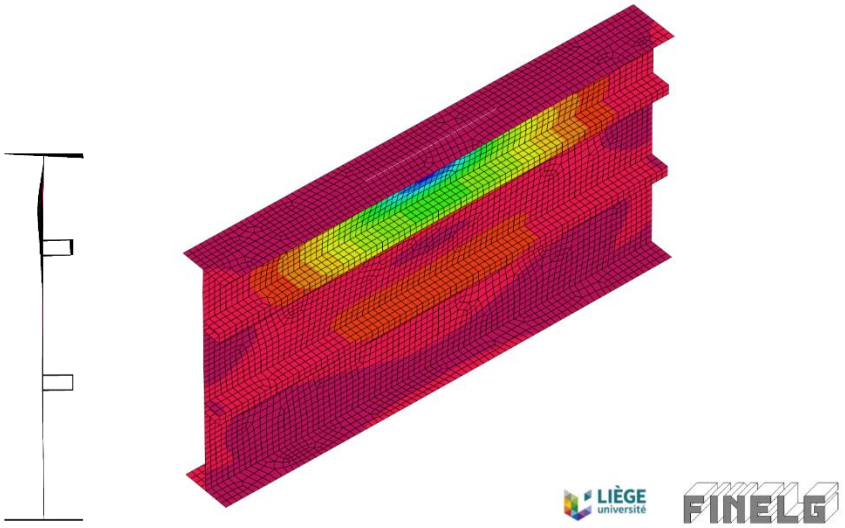

Figure 23: Interactive buckling; Seitz-2-hstw50 [15].

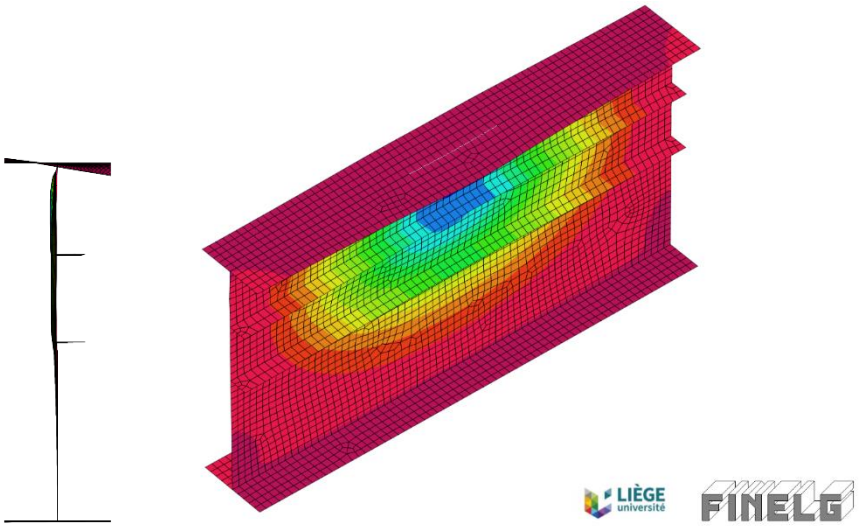

Figure 24: Global web buckling; Kövesdi-2-tw8 [15].

4.2 Models with open section stiffeners

4.2.1 Effect of the thickness of the longitudinal stiffener

For a single longitudinal stiffener, Figure 25 displays the comparison of the design method calculations and FEM analyses for an increasing stiffener thickness. The light green line indicates the EN1993-1-5 method and is significantly lower than Davaine's and Graciano's method, respectively the light blue and yellow lines. Doubling the thickness of a longitudinal stiffener does not result in a significant increase of patch loading resistance, as indicated by the nearly horizontal progression of the results. The same behaviour recurs for the configurations with two and three stiffeners, respectively represented by Figure 26 and Figure 27.

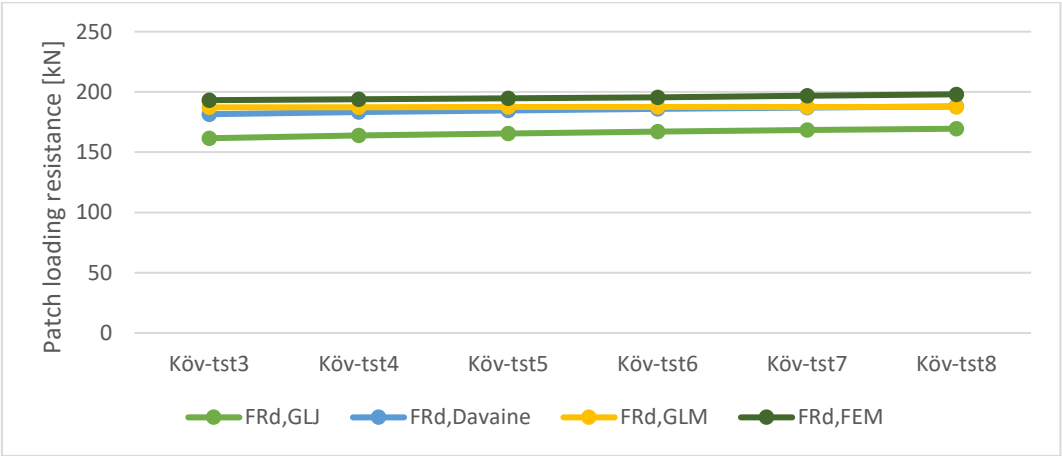

Figure 25: Comparison of the patch loading resistances for Kövesdi-1 when changing the thickness of the longitudinal stiffener.

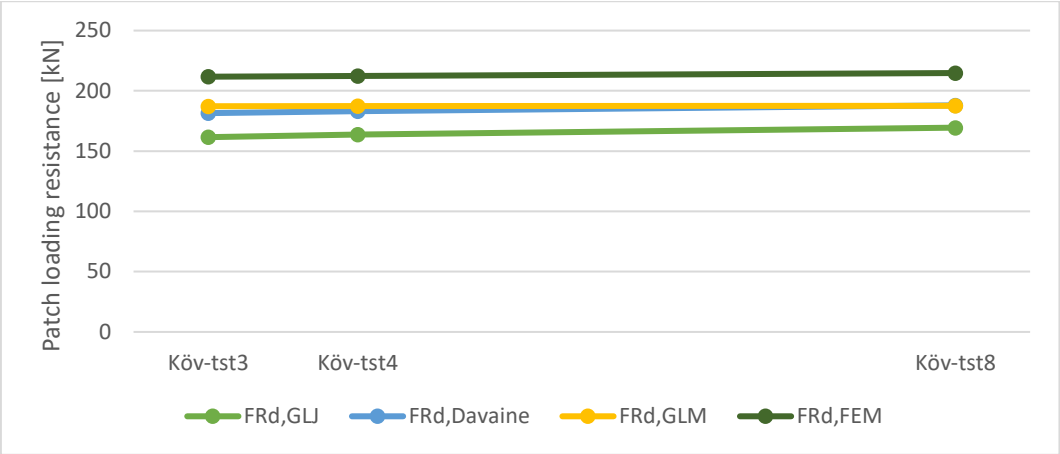

Figure 26: Comparison of the patch loading resistances for Kövesdi-2 when changing the thickness of the longitudinal stiffener.

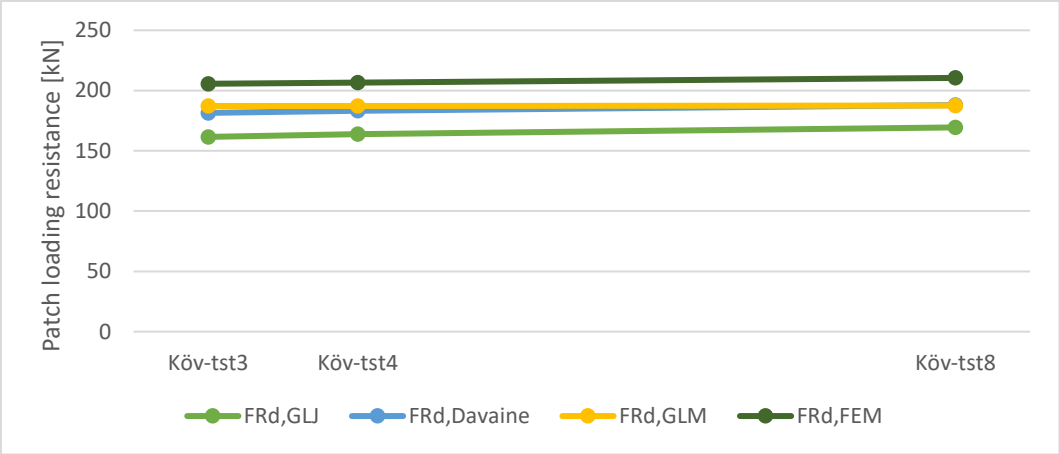

Figure 27: Comparison of the patch loading resistances for Kövesdi-3 when changing the thickness of the longitudinal stiffener.

When comparing the FEM results of the three stiffener configurations in Figure 28, the same nearly horizontal behaviour is present. The results of the configuration with two stiffeners are higher than the configuration with three stiffeners because by adding the third stiffener, local buckling of the subpanels was introduced and seemed more critical than the global buckling present in that specific section of the configuration with only two stiffeners.

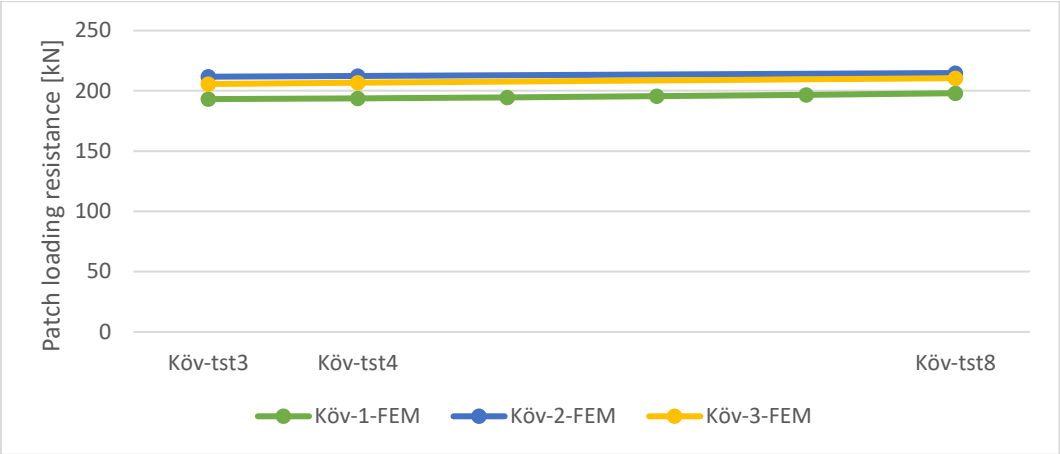

Figure 28: Comparison of the numerically calculated patch loading resistances for the three models when changing the thickness of the longitudinal stiffener.

4.2.2 Effect of the width of the longitudinal stiffener

Both EN1993-1-5 and Davaine's calculation methods result in a linear increase of the patch loading resistance when increasing the width of the longitudinal stiffener. FEM calculations and Graciano's improved formula have a similar behaviour but use a more conservative angle that leads in a nearly horizontal line. The configuration with two and three stiffeners share this behaviour. For the configuration with a single stiffener, due to the large imperfections that were applied, the last result of the FEM analysis falls short when compared to Davaine's method. This is displayed in Figure 29 through Figure 31.

The comparison of the three FEM analyses (Figure 32) shows a similar behaviour as discussed when changing the thickness of the longitudinal stiffener: in the configuration with three stiffeners, the local buckling of the subpanels seems to be more critical than the global buckling present in the configuration with two stiffeners.

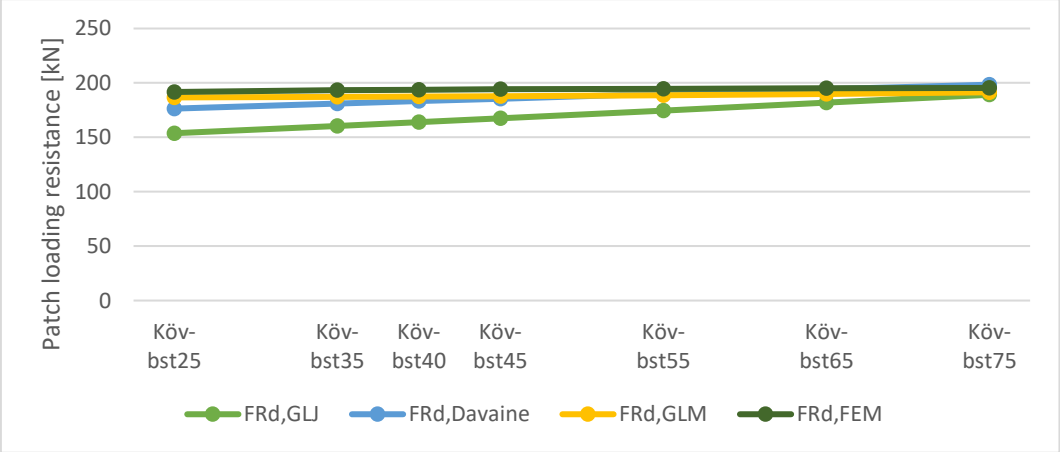

Figure 29: Comparison of the patch loading resistances for Kövesdi-1 when changing the width of the longitudinal stiffener.

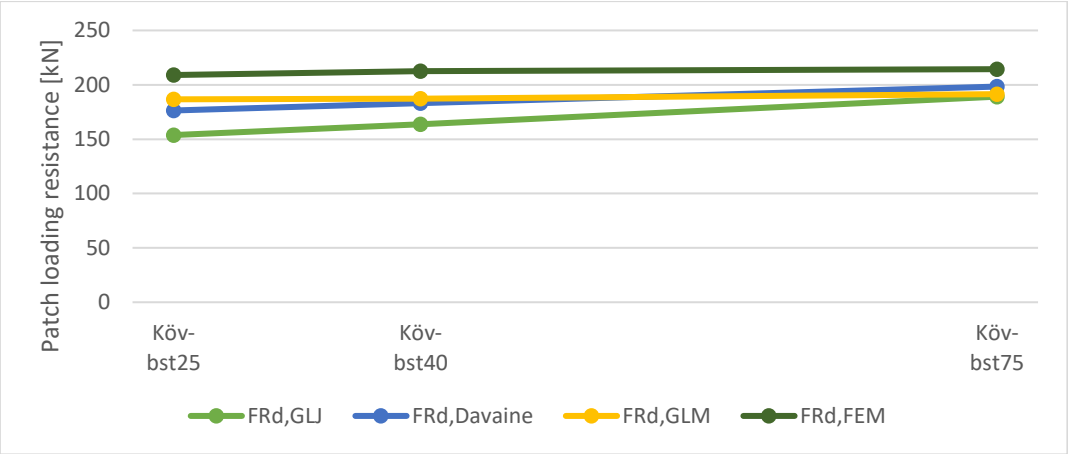

Figure 30: Comparison of the patch loading resistances for Kövesdi-2 when changing the width of the longitudinal stiffener.

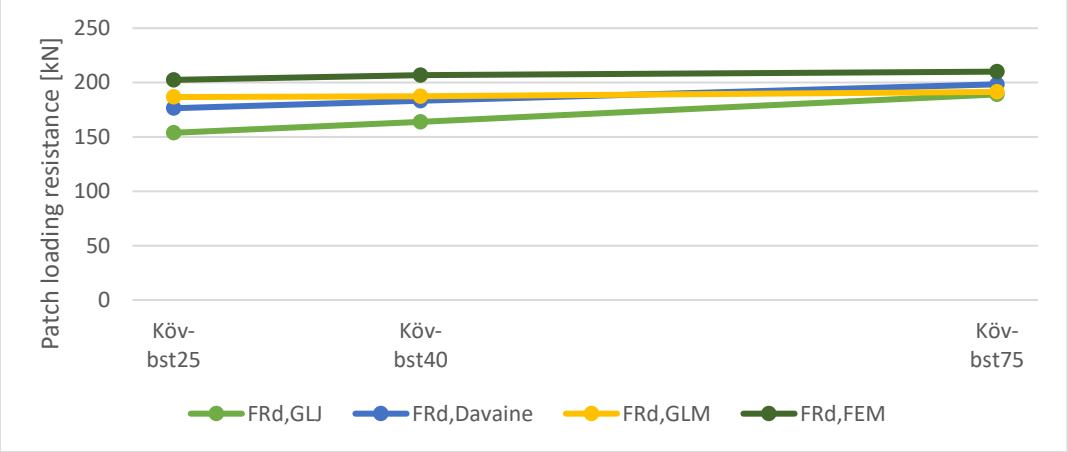

Figure 31: Comparison of the patch loading resistances for Kövesdi-3 when changing the width of the longitudinal stiffener.

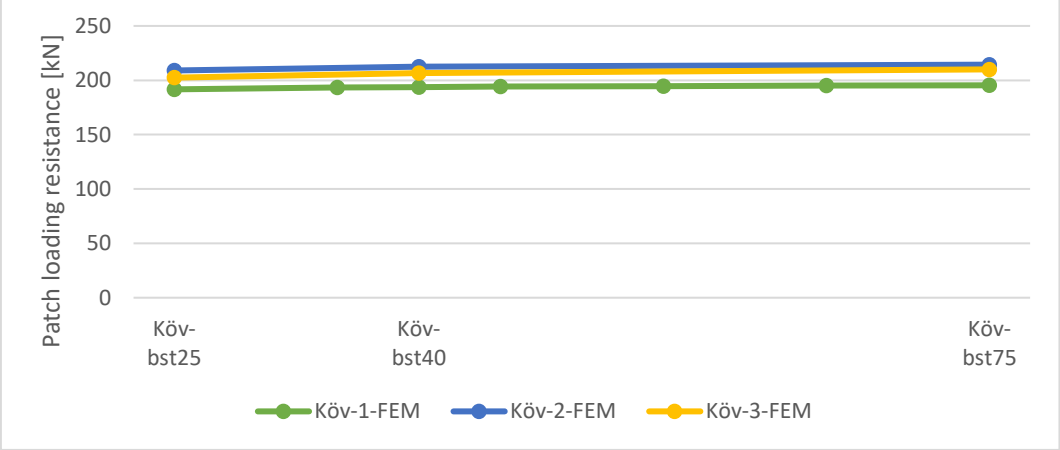

Figure 32: Comparison of the numerically calculated patch loading resistances for the three models when changing the width of the longitudinal stiffener.

4.2.3 Effect of the height of the upper subpanel

Figure 33 shows a dip in patch loading resistance across all but Graciano's calculation methods. This dip can be explained as a positive influence on the buckling shape of the subpanels. Positive here means that it helps to introduce the buckling. In general, stiffener placement remains key and should be tested thoroughly before being applied in praxis.

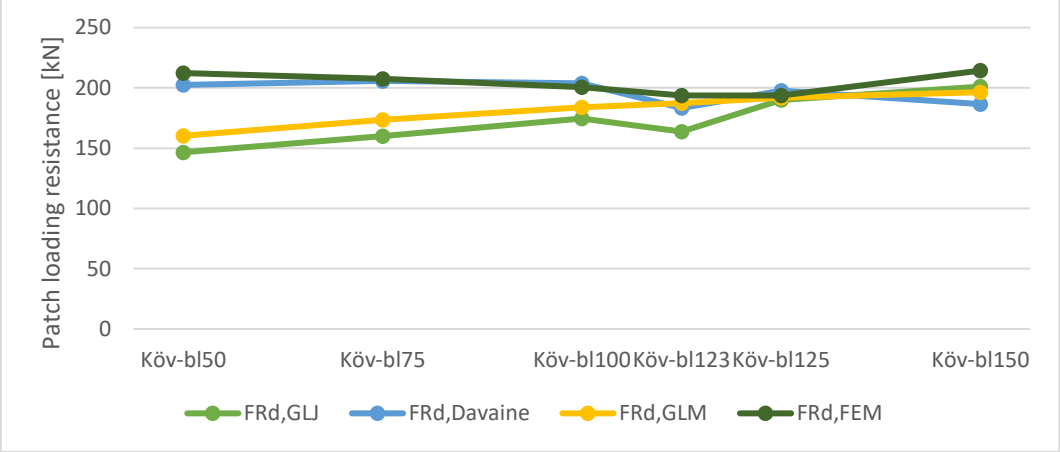

Figure 33: Comparison of the patch loading resistances for Kövesdi-1 when changing the height of the upper subpanel.

4.2.4 Effect of the loading length of the steel girder

Increasing the loading length of the steel girder also results in an increase in the patch loading resistance. This is true for all tested calculation methods and configurations. A nearly linear behaviour is displayed in Figure 34 through Figure 36. For configurations with one stiffener, the results from the FEM analyses continue to be almost equal to those of the design methods and proposals.

Figure 37 shows a similar behaviour as seen in the previous FEM comparisons where the patch loading resistance of the configuration with two stiffeners surpasses that of the one with three stiffeners. This happens due to the local instabilities induced by the application of the third stiffener.

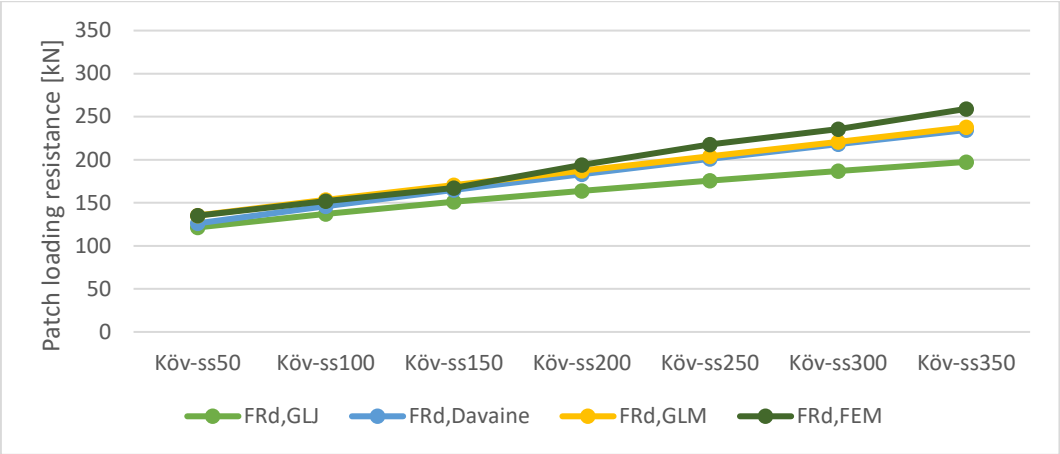

Figure 34: Comparison of the patch loading resistances for Kövesdi-1 when changing the loading length of the steel girder.

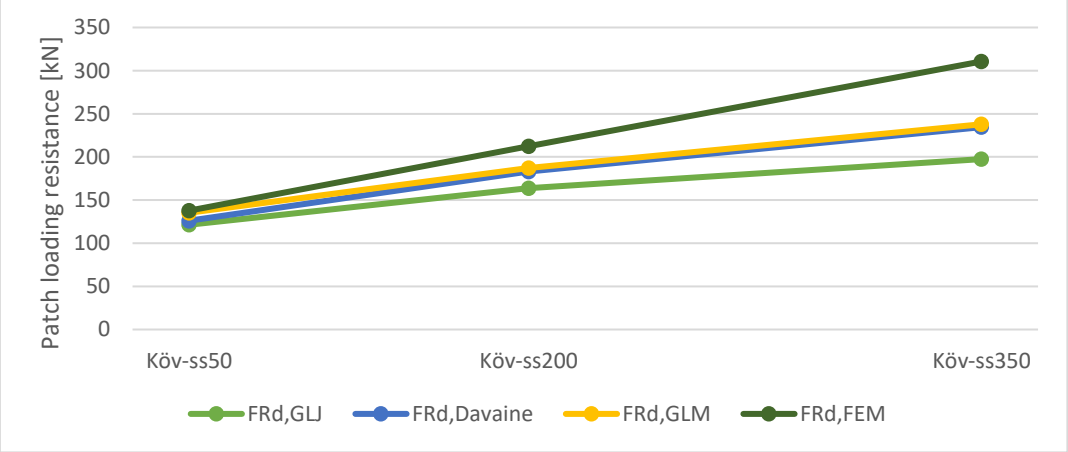

Figure 35: Comparison of the patch loading resistances for Kövesdi-2 when changing the loading length of the steel girder.

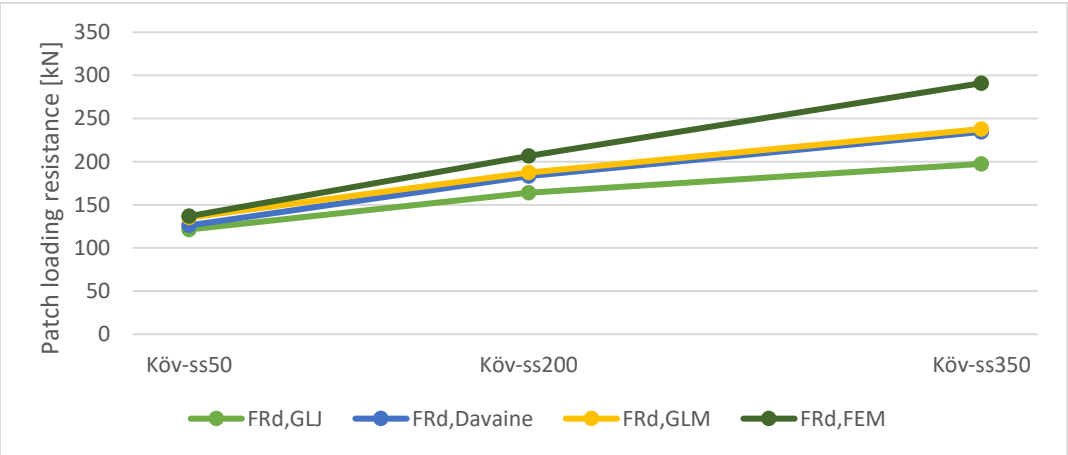

Figure 36: Comparison of the patch loading resistances for Kövesdi-3 when changing the loading length of the steel girder.

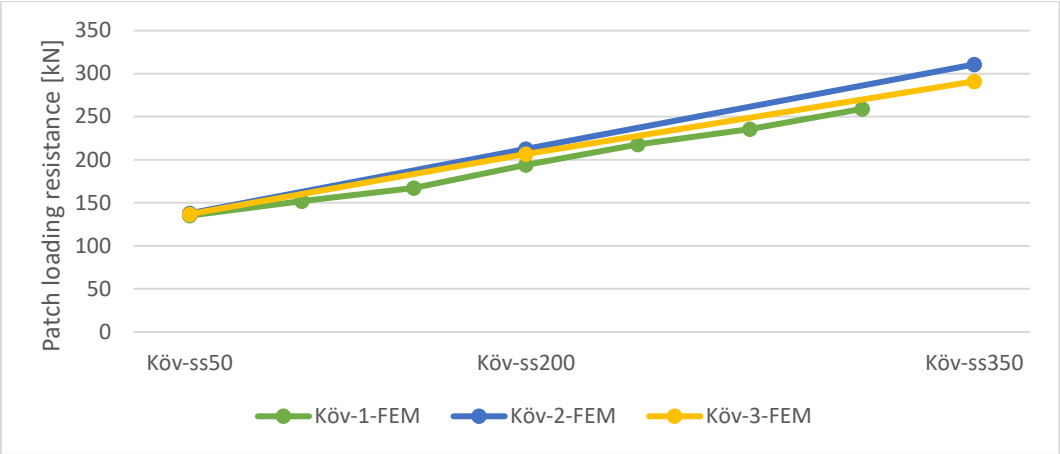

Figure 37: Comparison of the numerically calculated patch loading resistances for the three models when changing the loading length of the steel girder.

4.2.5 Effect of the thickness of the girder web

Increasing the thickness of the girder web results in the most significant gains in patch loading resistance, as doubling the web thickness more than doubles the total patch loading resistance. Figure 38 until Figure 40 show an almost identical linear to slightly exponential line for Davaine's and Graciano's calculation methods.

Figure 41 shows that, for open section stiffeners, it no longer matters whether one, two or three stiffeners are applied as the stiffeners become too weak to have any noteworthy effect.

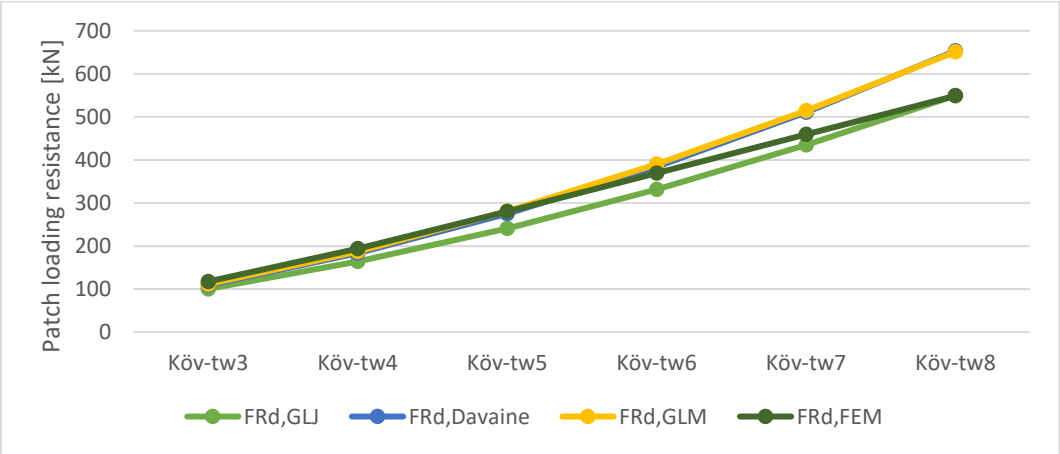

Figure 38: Comparison of the patch loading resistances for Kövesdi-1 when changing the thickness of the girder web.

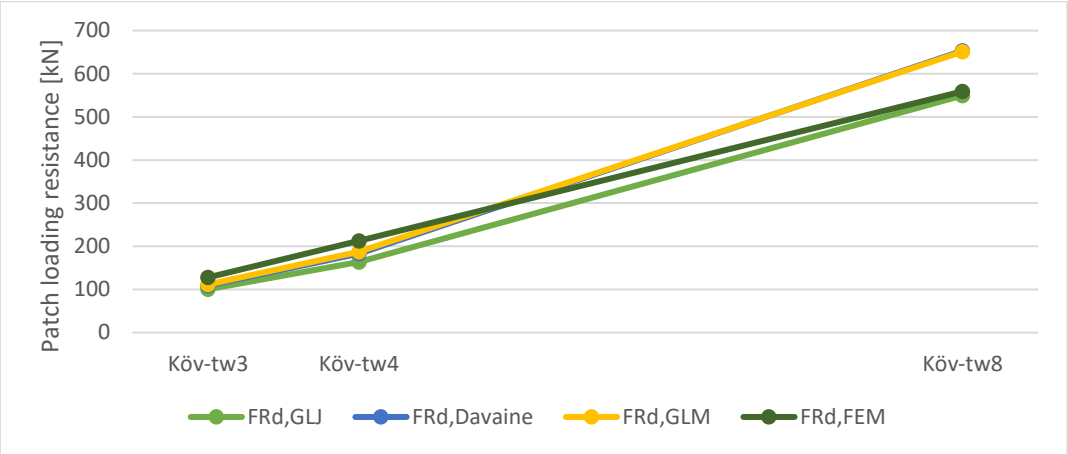

Figure 39: Comparison of the patch loading resistances for Kövesdi-2 when changing the thickness of the girder web.

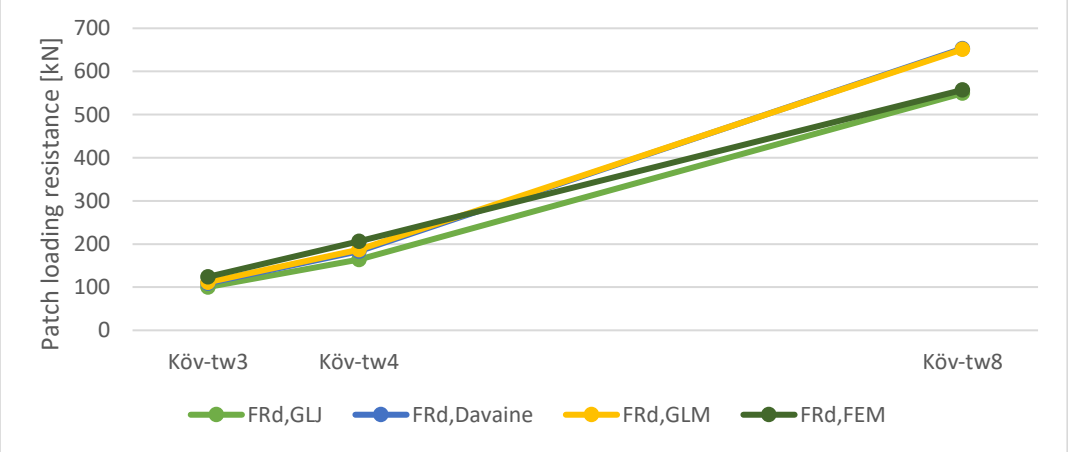

Figure 40: Comparison of the patch loading resistances for Kövesdi-3 when changing the thickness of the girder web.

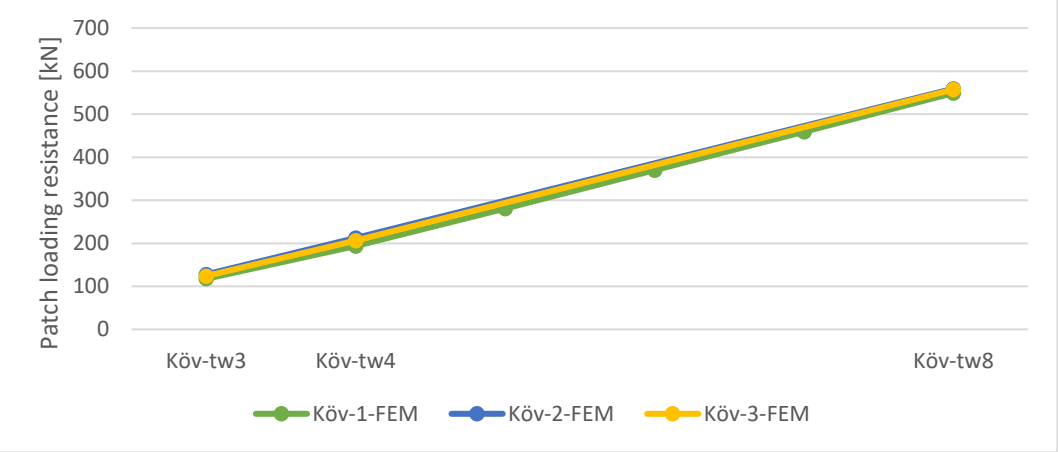

Figure 41: Comparison of the numerically calculated patch loading resistances for the three models when changing the thickness of the girder web.

4.3 Models with closed section stiffeners

4.3.1 Effect of the thickness of the longitudinal stiffener

Increasing the thickness of the longitudinal stiffener does not lead to a significant increase in patch loading, just like it did not for open section stiffeners. The same behaviour recurs when doubling the stiffeners' thickness: this yields hardly any increase in patch loading resistance. When compared to the configurations with the open section stiffeners, the difference is that FEM analysis proves the actual resistance is significantly underestimated by both the EN1993-1-5 and the improved calculation methods, and this even despite having an exaggerated imperfection. Figure 42 shows this for the configurations with a single stiffener, while Figure 43 does this for the configuration with two longitudinal stiffeners. The EN1993-1-5 is indicated in light green, Davaine's improved method in light blue, Graciano's in yellow and finally the FEM analysis is represented by the dark green colour.

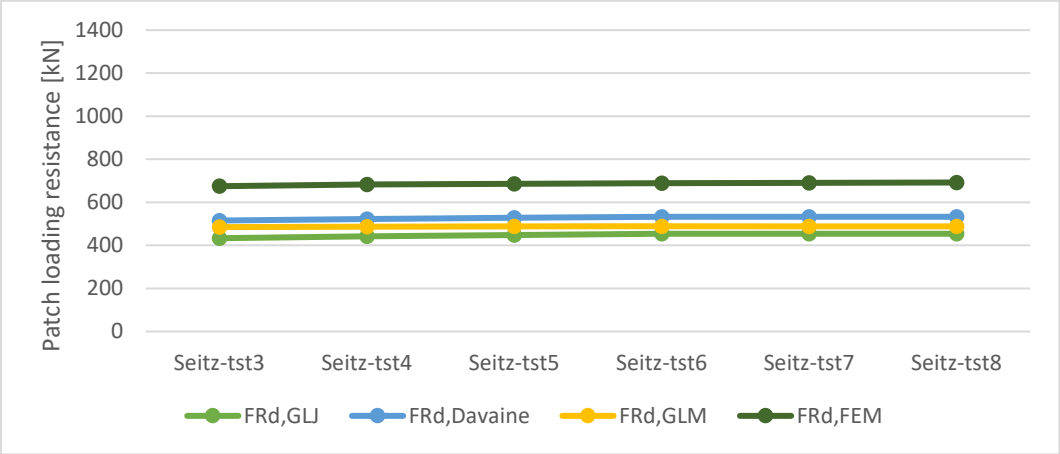

Figure 42: Comparison of the patch loading resistances for Seitz-1 when changing the thickness of the longitudinal stiffener.

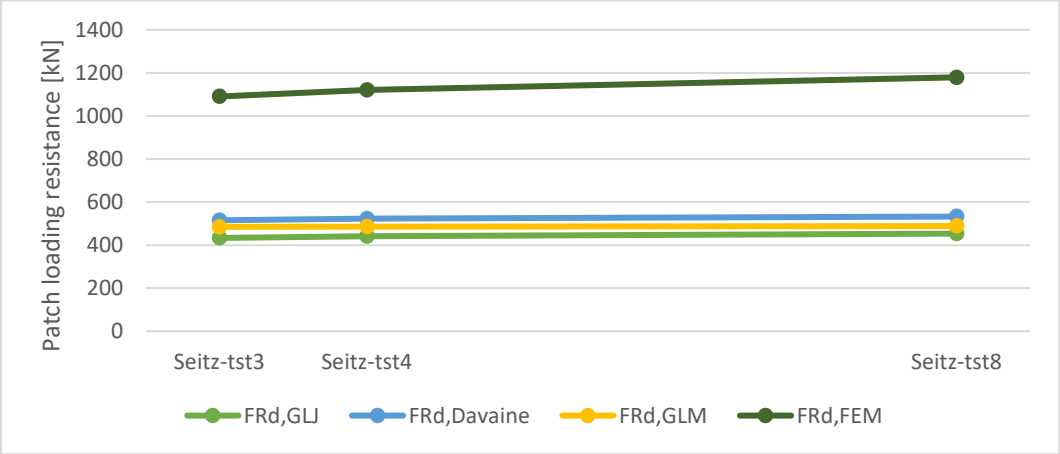

Figure 43: Comparison of the patch loading resistances for Seitz-2 when changing the thickness of the longitudinal stiffener.

Figure 44 compares the FEM results for the two stiffener configurations. The same behaviour recurs: a nearly horizontal line indicating a small increase in patch loading resistance.

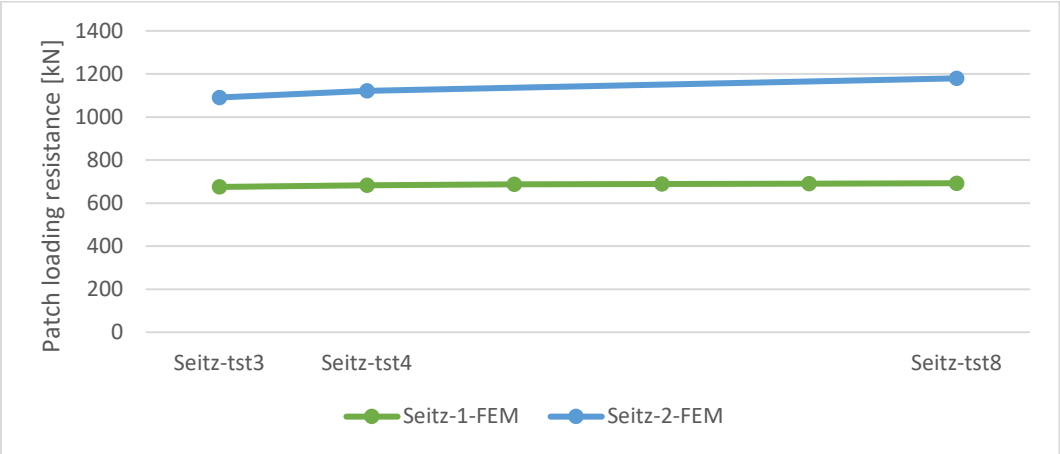

Figure 44: Comparison of the numerically calculated patch loading resistances for the two models when changing the thickness of the longitudinal stiffener.

4.3.2 Effect of the width of the longitudinal stiffener

Figure 45 displays a seemingly maximum value for the calculation methods and proposals that is reached around the configuration with a stiffener width of 120 mm (20 mm more than the basic model). The three calculation methods (EN1993-1-5, Davaine, and Graciano et al.) continue increasing until this configuration and then level out to a nearly horizontal line. Graciano's improved proposal also shows this behaviour, albeit in a less pronounced manner. This is due to the maximum stiffeners' stiffness that has been reached, as described in Formula 28. Looking at the FEM results, a similar pattern seems to occur due to the minimal increments and this confirms the approximation of a maximum stiffeners' stiffness. A similar behaviour can be assumed in Figure 46, however, more reference points should be tested to say this with complete certainty. The latter also applies when comparing the results of both FEM analyses. In general, the figures depict a significant underestimation of the patch loading resistance that only becomes more apparent when multiple stiffeners are applied.

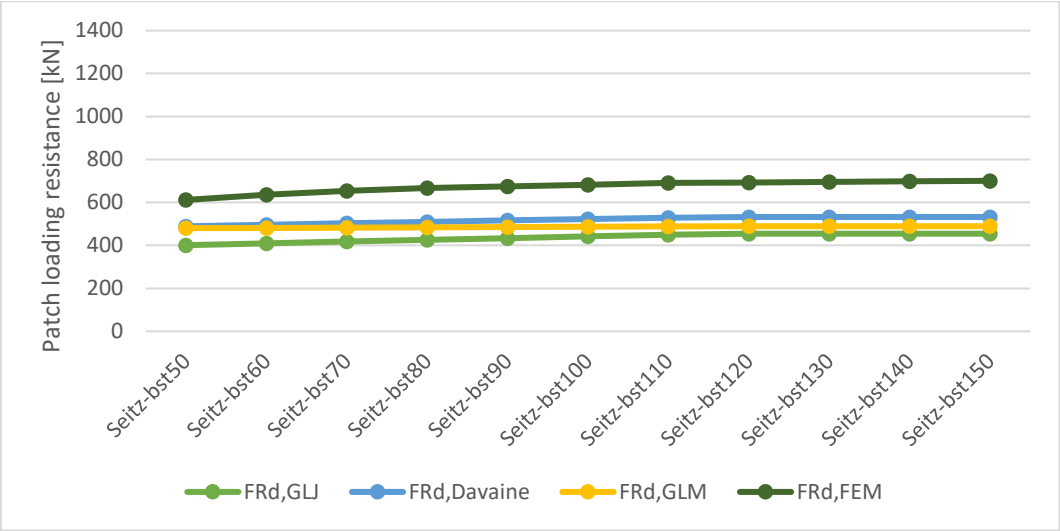

Figure 45: Comparison of the patch loading resistances for Seitz-1 when changing the width of the longitudinal stiffener.

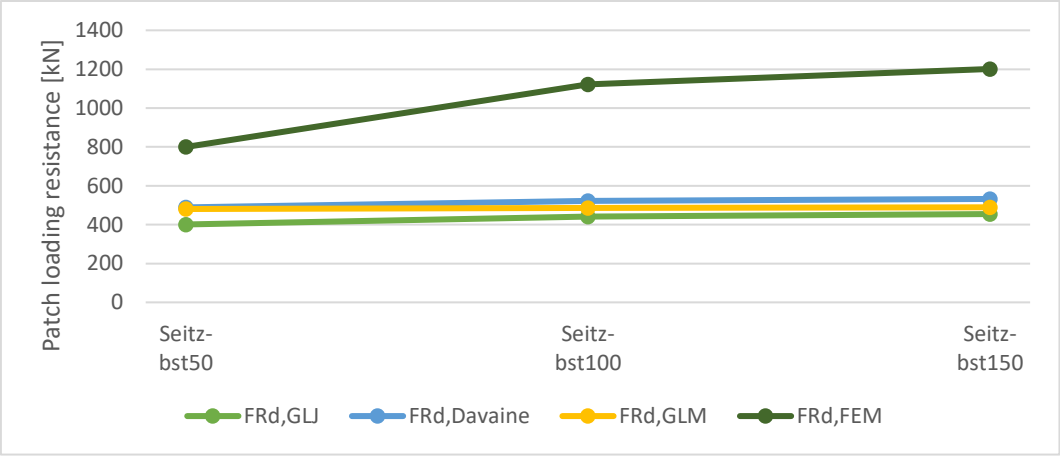

Figure 46: Comparison of the patch loading resistances for Seitz-2 when changing the width of the longitudinal stiffener.

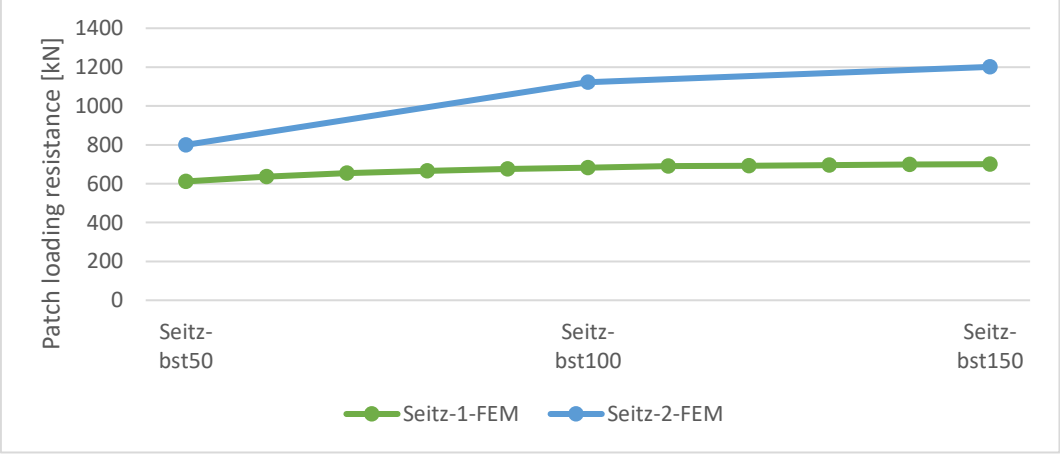

Figure 47: Comparison of the numerically calculated patch loading resistances for the two models when changing the width of the longitudinal stiffener.

4.3.3 Effect of the outer height of the longitudinal stiffener

Figure 48 through Figure 50 show a nearly horizontal progression when increasing the outer height of the longitudinal stiffener for all of the calculation methods and proposals, but also for the FEM analyses. The underestimation of the patch loading resistance by the existing calculation methods and proposals recurs and this continues to be the trend in all further cases.

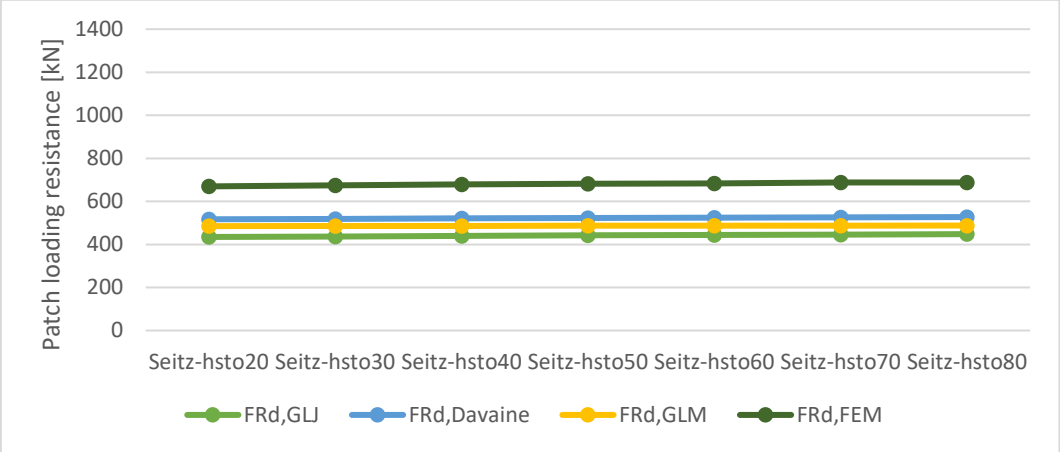

Figure 48: Comparison of the patch loading resistances for Seitz-1 when changing the outer height of the longitudinal stiffener.

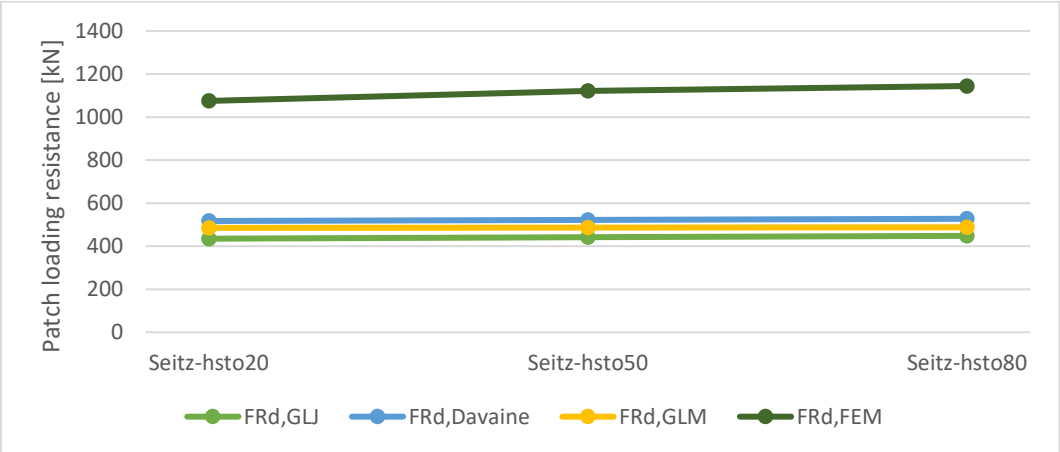

Figure 49: Comparison of the patch loading resistances for Seitz-2 when changing the outer height of the longitudinal stiffener.

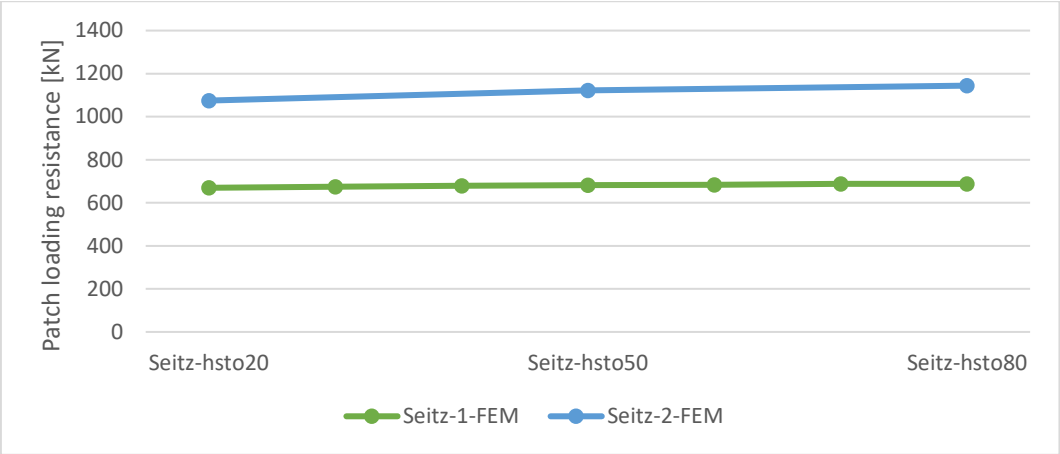

Figure 50: Comparison of the numerically calculated patch loading resistances for the two models when changing the outer height of the longitudinal stiffener.

4.3.4 Effect of the inner height of the longitudinal stiffener

Unlike the outer height of the longitudinal stiffener, the inner height does improve the patch loading resistance according to Davaine's calculation method and the FEM analyses. EN1993-1-5 and Graciano's methods, however, present a decreasing resistance (Figure 51). A similar behaviour occurs for the configurations with two stiffeners (Figure 52 and Figure 53).

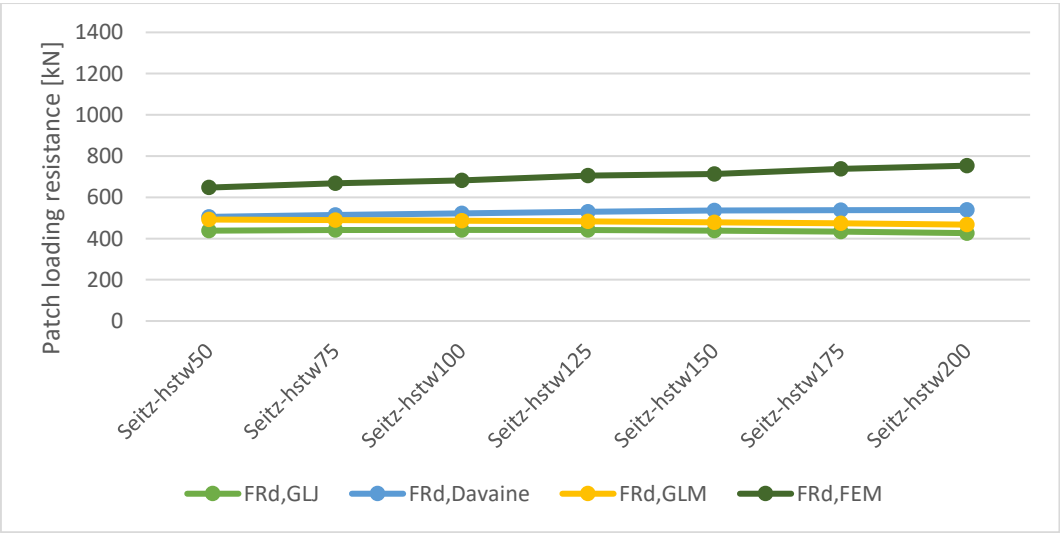

Figure 51: Comparison of the patch loading resistances for Seitz-1 when changing the inner height of the longitudinal stiffener.

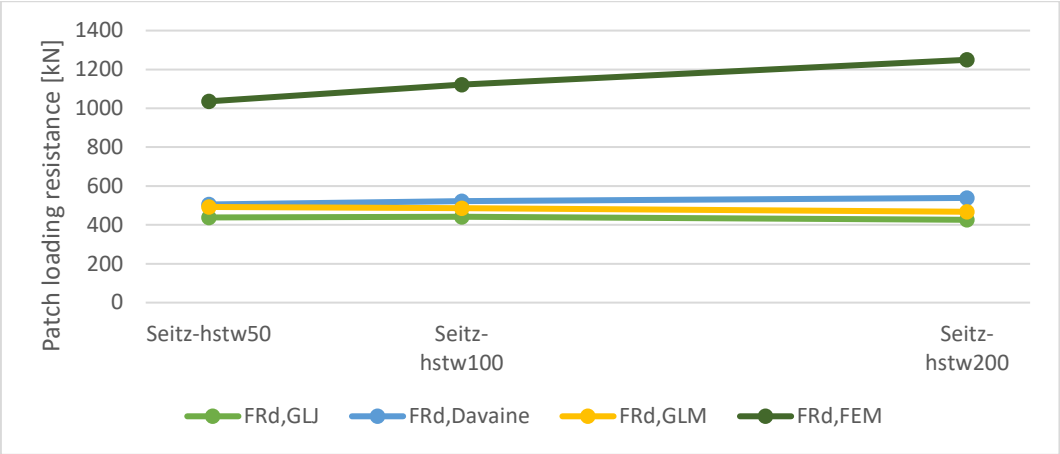

Figure 52: Comparison of the patch loading resistances for Seitz-2 when changing the inner height of the longitudinal stiffener.

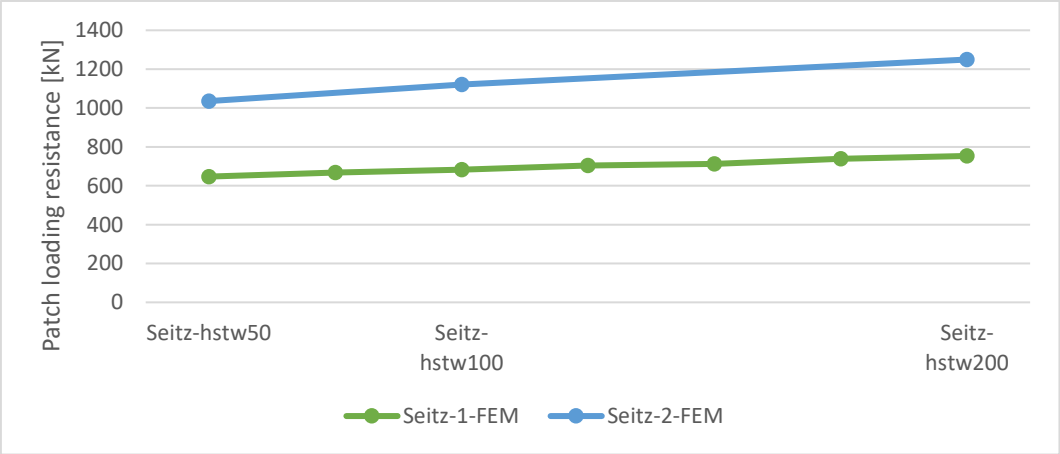

Figure 53: Comparison of the numerically calculated patch loading resistances for the two models when changing the inner height of the longitudinal stiffener.

4.3.5 Effect of the height of the upper subpanel

For the calculation methods and proposals, Figure 54 exhibits a set of curved lines that seemingly converge around an upper subpanel height of 320 mm. Davaine's proposal is somewhat more accurate because it includes factors to take the subpanel buckling into account, yet it still largely underestimates the patch loading resistance. The FEM results decrease when the height of the upper subpanel increases, until a height of 280 mm. This is due to the subpanel height having a positive influence on the propagation of local instabilities.

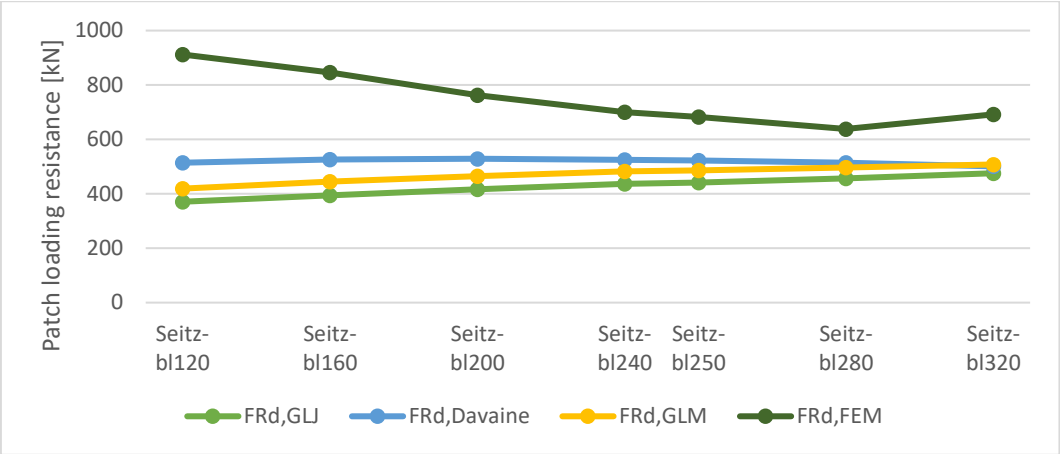

Figure 54: Comparison of the patch loading resistances for Seitz-1 when changing the height of the upper subpanel.

4.3.6 Effect of the loading length of the steel girder

For short loading lengths, the calculation methods and proposals are a valid option to calculate patch loading resistance. However, like Figure 55 depicts, the longer the loading length, the more the patch loading resistances disseminate. The four sets of results show a similar nearly linear behaviour, albeit with a different angle. The patch loading resistance is underestimated more with a longer loading length. This pattern is also visible in Figure 56 and Figure 57 for, respectively, the configuration with two longitudinal stiffeners applied on the steel girder web, and the comparison of the FEM results.

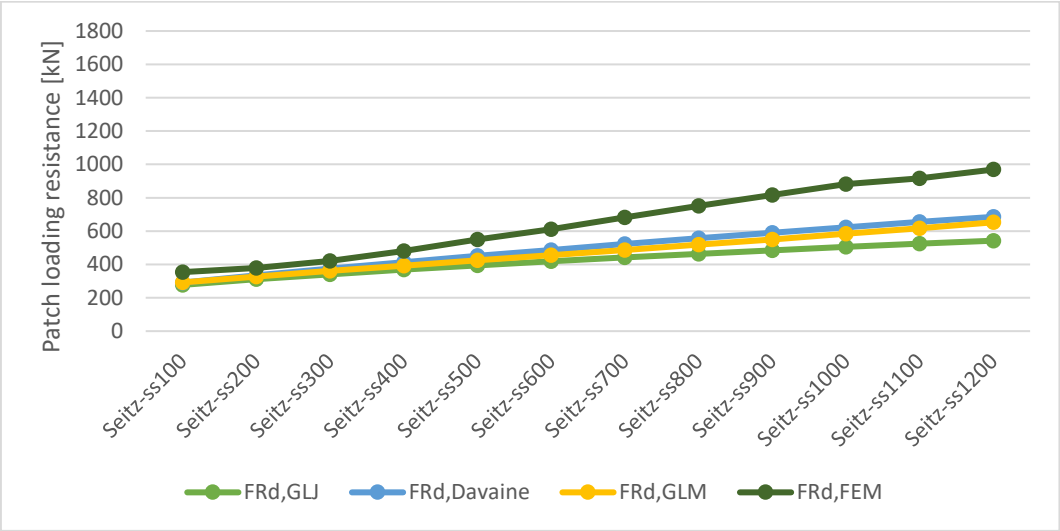

Figure 55: Comparison of the patch loading resistances for Seitz-1 when changing the loading length of the steel girder.

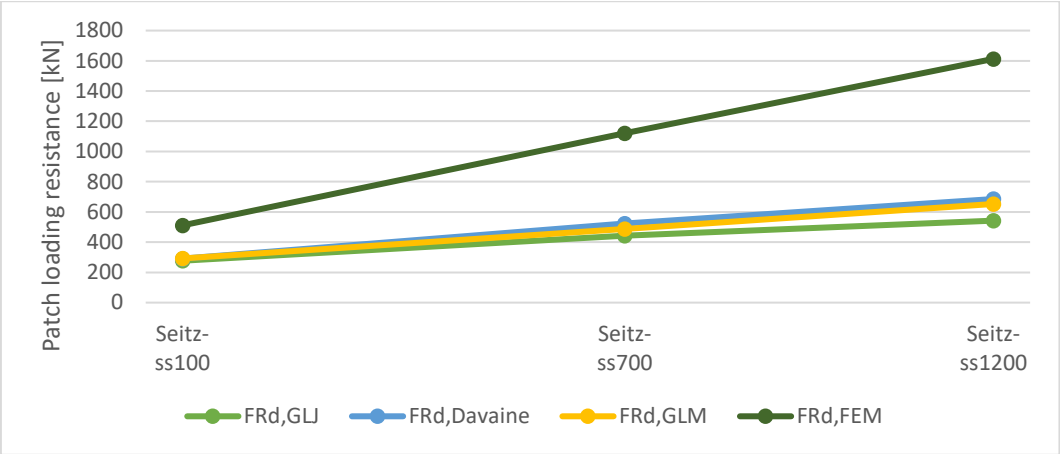

Figure 56: Comparison of the patch loading resistances for Seitz-2 when changing the loading length of the steel girder.

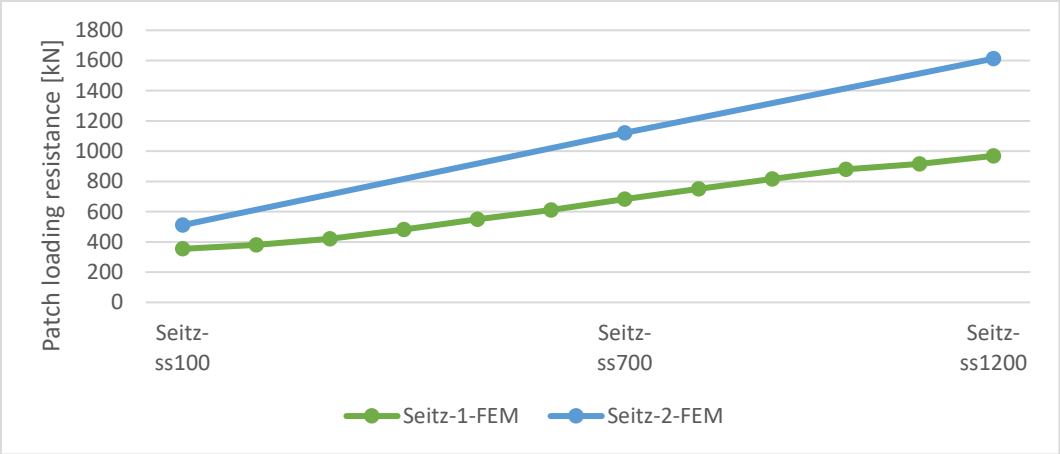

Figure 57: Comparison of the numerically calculated patch loading resistances for the two models when changing the loading length of the steel girder.

4.3.7 Effect of the thickness of the girder web

Increasing the thickness of the girder web results in the most significant gains in patch loading resistance, as doubling the web thickness more than doubles the total patch loading resistance. The results disseminate further when a thicker girder web is applied. This is visible in Figure 58 and Figure 59. Davaine's calculation method is, again, the more accurate option out of the calculation methods and proposals. When comparing the FEM results in Figure 60, the increase in patch loading resistance is more pronounced in the configuration with two stiffeners than it is in the one with a single longitudinal stiffener. This is due to a negative influence on the propagation of instabilities.

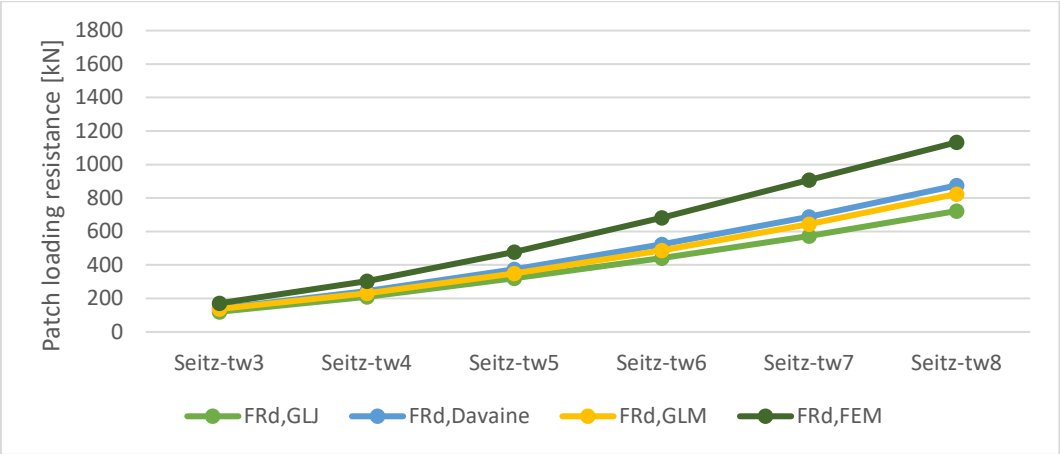

Figure 58: Comparison of the patch loading resistances for Seitz-1 when changing the thickness of the girder web.

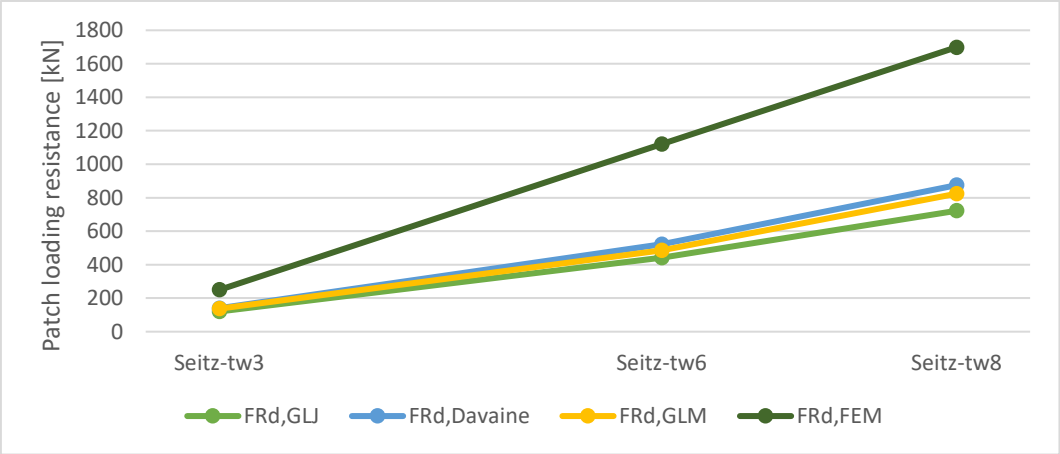

Figure 59: Comparison of the patch loading resistances for Seitz-2 when changing the thickness of the girder web.

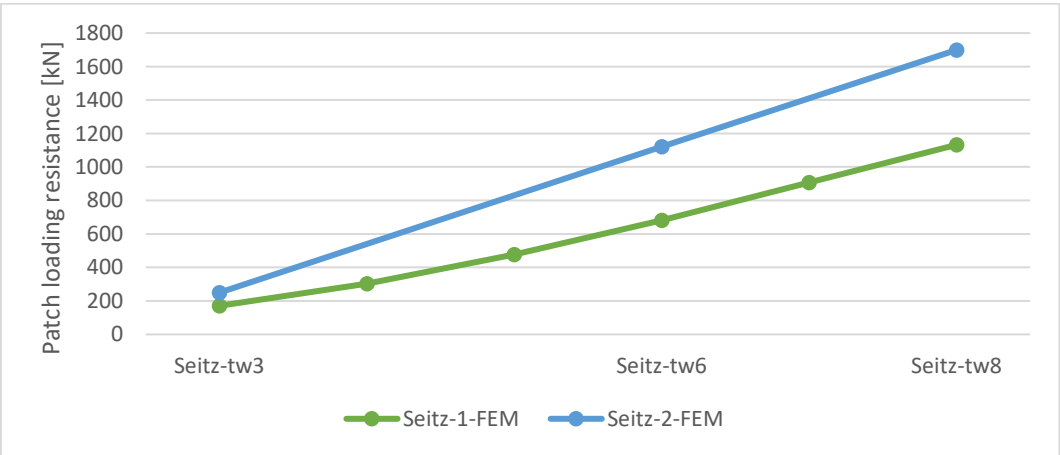

Figure 60: Comparison of the numerically calculated patch loading resistances for the two models when changing the thickness of the girder web.

5 Summary and conclusions

This paper compares the patch loading resistance of existing analytical design methods and numerical analyses. The structural behaviour of steel I-section girders with varying configuration and numbers of longitudinal stiffeners are studied, and the calculated patch loading resistances are compared. It can be concluded that for girders with single open section stiffeners, Graciano's design proposal [14] seems to be the more accurate analytical calculation method in most cases. The analytical formulas do not properly take multiple stiffeners into account. As a result, the patch loading resistance is underestimated in case of both open section and also closed section stiffeners. The patch loading resistance of steel girders with a single closed section girder is also underestimated. When compared to the other tested design methods and proposals, Davaine's proposal [5] is the more accurate option for closed stiffeners.

Applying an extra stiffener may have a negative effect on the patch loading resistance, as a different and more critical buckling behaviour can be introduced. In case of longitudinally stiffened girders with either open or closed section stiffeners, increasing the thickness of the web (t_w) has a significant effect. Increasing the thickness of the girder web also reduces the relative stiffness of the stiffeners and will result in the stiffeners having a reduced effect on the patch loading resistance, as presented in Figure 38 until Figure 41. On the other hand, increasing the thickness of the stiffeners (t_{st}) has little effect on the patch loading resistance. Changing the position of the only stiffener can result in drastic changes to the patch loading resistance. Although the results of the numerical and analytical calculations scatter, they all prove that increasing the loading length improves the patch loading resistance. According to the FEM analyses, increasing the width of the stiffener (b_{st}) has little to no effect beyond a certain point. This corresponds with the already available relative flexural rigidity of the longitudinal stiffener (γ_s) that reaches a certain limit value in the analytical calculations [6]. Lastly, adapting the outer height of a closed stiffener ($h_{st,o}$) has little effect on the patch loading resistance. Increasing its inner height ($h_{st,w}$), however, does improve the patch loading resistance.

As proven by this study, the available analytical methods of calculating the patch loading resistance of longitudinally stiffener steel girders needs improvement. The patch loading resistance is underestimated in most cases, safe the tested configurations with a single open section stiffener. This underestimation becomes more significant whenever multiple stiffeners are applied.

List of references

[1] B. Paulmac, Artist, *Incremental launching.* [Art]. Wikimedia Commons, 2014.

[2] B. Kövesdi, "Patch loading resistance of slender plate girders with longitudinal stiffeners," *Journal of Constructional Steel Research,* vol. 140, pp. 237-246, 2018.

[3] M. Clarin, Plate Buckling Resistance - Patch Loading of Longitudinally Stiffened Webs and Local Buckling [PhD Thesis], Luleå: Luleå University of Technology, 2007.

[4] B. Kövesdi, B. Mecséri and L. Dunai, "Imperfection analysis on the patch loading resistance of girders with open section longitudinal stiffeners," *Thin-Walled Structures,* vol. 123, pp. 195-205, 2018.

[5] L. Davaine, Formulation de la résistance au lancement d'une âme métallique de pontraidie longitudinalement [Doctoral Thesis], Rennes, France: INSA de Rennes, 2005.

[6] EN1993-1-5:2006, "Eurocode 3 - Design of steel structures - Part 1.5: Plated structural elements," CEN, European Committee for Standardisation, Brussels, Belgium, 2013.

[7] M. Clarin, Plate Buckling Resistance - Patch Loading of Longitudinally Stiffened Webs and Local Buckling [Doctoral Thesis], Luleå, Sweden: Luleå University of Technology, 2007.

[8] M. Seitz, Tragverhalten längsversteifter Blechträger unter quergerichteter Krafteinleitung [Doctoral Thesis], Stuttgart: Institut für Konstruktion und Entwurf der Universität Stuttgart, 2005.

[9] C. Graciano, "Patch loading resistance of longitudinally stiffened girders – A systematic review," *Thin-Walled Structures,* vol. 95, pp. 1-6, 2015.

[10] A. Bergfelt, Patch loading on a slender web - Influence of horizontal and vertical web stiffeners on the load carrying capacity, Gothenburg, Sweden: Chalmers University of Technology, 1979.

[11] C. Graciano, Patch loading - Resistance of longitudinally stiffened steel girder webs [Doctoral thesis], Luleå, Sweden: Luleå University of Technology, 2002.

[12] N. Marković and N. Hajdin, "A contribution to the analysis of the behaviour of plate girders subjected to patch loading," *Journal of Constructional Steel Research,* vol. 21, no. 1-3, pp. 163-173, 1992.

[13] I. Kutmanová and M. Škaloud, "Ultimate limit state of slender steel webs subject to (i) constant and (ii) repeated partial edge loading," *Journal of Constructional Steel Research,* vol. 21, no. 1-3, pp. 147-162, 1992.

[14] C. Graciano and J. Mendes, "Elastic buckling of longitudinally stiffened patch loaded plate girders using factorial design," *Journal of Constructional Steel Research,* vol. 100, no. 1, pp. 229-236, 2014.

[15] UEE - ULiège, Engineering Office GREISCH, "FINELG - Nonlinear Finite Element Analysis Program," UEE - ULiège, Engineering Office GREISCH, Liège, 2019.

Appendices

Appendix A List of analysed models

Table 6: Complete list on analysed models with parameters.

Specimen	t_w	a	h_w	f_{yw}	t_f	b_f	f_{yf}	s_s	b_l	t_{st}	$h_{st,o}$	$h_{st,w}$	b_{st}
Kövesdi-1	4	1000	500	355	10	150	355	200	123	4	0	0	40
Kövesdi-1-tst3	4	1000	500	355	10	150	355	200	123.5	3	0	0	40
Kövesdi-1-tst5	4	1000	500	355	10	150	355	200	122.5	5	0	0	40
Kövesdi-1-tst6	4	1000	500	355	10	150	355	200	122	6	0	0	40
Kövesdi-1-tst7	4	1000	500	355	10	150	355	200	121.5	7	0	0	40
Kövesdi-1-tst8	4	1000	500	355	10	150	355	200	121	8	0	0	40
Kövesdi-1-bst25	4	1000	500	355	10	150	355	200	123	4	0	0	25
Kövesdi-1-bst35	4	1000	500	355	10	150	355	200	123	4	0	0	35
Kövesdi-1-bst45	4	1000	500	355	10	150	355	200	123	4	0	0	45
Kövesdi-1-bst55	4	1000	500	355	10	150	355	200	123	4	0	0	55
Kövesdi-1-bst65	4	1000	500	355	10	150	355	200	123	4	0	0	65
Kövesdi-1-bst75	4	1000	500	355	10	150	355	200	123	4	0	0	75
Kövesdi-1-bl50	4	1000	500	355	10	150	355	200	50	4	0	0	60
Kövesdi-1-bl75	4	1000	500	355	10	150	355	200	75	4	0	0	65
Kövesdi-1-bl100	4	1000	500	355	10	150	355	200	100	4	0	0	70
Kövesdi-1-bl125	4	1000	500	355	10	150	355	200	125	4	0	0	75
Kövesdi-1-bl150	4	1000	500	355	10	150	355	200	150	4	0	0	75
Kövesdi-1-ss50	4	1000	500	355	10	150	355	50	123	4	0	0	40
Kövesdi-1-ss100	4	1000	500	355	10	150	355	100	123	4	0	0	40
Kövesdi-1-ss150	4	1000	500	355	10	150	355	150	123	4	0	0	40
Kövesdi-1-ss250	4	1000	500	355	10	150	355	250	123	4	0	0	40

Specimen	t_w	a	h_w	f_{yw}	t_f	b_f	f_{yf}	s_s	b_l	t_{st}	$h_{st,o}$	$h_{st,w}$	b_{st}
Kövesdi-1-ss300	4	1000	500	355	10	150	355	300	123	4	0	0	40
Kövesdi-1-ss350	4	1000	500	355	10	150	355	350	123	4	0	0	40
Kövesdi-1-tw3	3	1000	500	355	10	150	355	200	123	4	0	0	40
Kövesdi-1-tw5	5	1000	500	355	10	150	355	200	123	4	0	0	40
Kövesdi-1-tw6	6	1000	500	355	10	150	355	200	123	4	0	0	40
Kövesdi-1-tw7	7	1000	500	355	10	150	355	200	123	4	0	0	40
Kövesdi-1-tw8	8	1000	500	355	10	150	355	200	123	4	0	0	40
Kövesdi-2	4	1000	500	355	10	150	355	200	123	4	0	0	40
Kövesdi-2-tst3	4	1000	500	355	10	150	355	200	123.5	3	0	0	40
Kövesdi-2-tst8	4	1000	500	355	10	150	355	200	121	8	0	0	40
Kövesdi-2-bst25	4	1000	500	355	10	150	355	200	123	4	0	0	25
Kövesdi-2-bst75	4	1000	500	355	10	150	355	200	123	4	0	0	75
Kövesdi-2-ss50	4	1000	500	355	10	150	355	50	123	4	0	0	40
Kövesdi-2-ss350	4	1000	500	355	10	150	355	350	123	4	0	0	40
Kövesdi-2-tw3	3	1000	500	355	10	150	355	200	123	4	0	0	40
Kövesdi-2-tw8	8	1000	500	355	10	150	355	200	123	4	0	0	40
Kövesdi-3	4	1000	500	355	10	150	355	200	123	4	0	0	40
Kövesdi-3-tst3	4	1000	500	355	10	150	355	200	123.5	3	0	0	40
Kövesdi-3-tst8	4	1000	500	355	10	150	355	200	121	8	0	0	40
Kövesdi-3-bst25	4	1000	500	355	10	150	355	200	123	4	0	0	25
Kövesdi-3-bst75	4	1000	500	355	10	150	355	200	123	4	0	0	75
Kövesdi-3-ss50	4	1000	500	355	10	150	355	50	123	4	0	0	40
Kövesdi-3-ss350	4	1000	500	355	10	150	355	350	123	4	0	0	40
Kövesdi-3-tw3	3	1000	500	355	10	150	355	200	123	4	0	0	40
Kövesdi-3-tw8	8	1000	500	355	10	150	355	200	123	4	0	0	40

Specimen	t_w	a	h_w	f_{yw}	t_f	b_f	f_{yf}	s_s	b_l	t_{st}	$h_{st,o}$	$h_{st,w}$	b_{st}
Seitz-1	6	2400	1200	355	20	260	355	700	250	4	50	100	100
Seitz-1-tst3	6	2400	1200	355	20	260	355	700	250.5	3	50	100	100
Seitz-1-tst5	6	2400	1200	355	20	260	355	700	249.5	5	50	100	100
Seitz-1-tst6	6	2400	1200	355	20	260	355	700	249	6	50	100	100
Seitz-1-tst7	6	2400	1200	355	20	260	355	700	248.5	7	50	100	100
Seitz-1-tst8	6	2400	1200	355	20	260	355	700	248	8	50	100	100
Seitz-1-bst50	6	2400	1200	355	20	260	355	700	250	4	50	100	50
Seitz-1-bst60	6	2400	1200	355	20	260	355	700	250	4	50	100	60
Seitz-1-bst70	6	2400	1200	355	20	260	355	700	250	4	50	100	70
Seitz-1-bst80	6	2400	1200	355	20	260	355	700	250	4	50	100	80
Seitz-1-bst90	6	2400	1200	355	20	260	355	700	250	4	50	100	90
Seitz-1-bst110	6	2400	1200	355	20	260	355	700	250	4	50	100	110
Seitz-1-bst120	6	2400	1200	355	20	260	355	700	250	4	50	100	120
Seitz-1-bst130	6	2400	1200	355	20	260	355	700	250	4	50	100	130
Seitz-1-bst140	6	2400	1200	355	20	260	355	700	250	4	50	100	140
Seitz-1-bst150	6	2400	1200	355	20	260	355	700	250	4	50	100	150
Seitz-1-hsto20	6	2400	1200	355	20	260	355	700	250	4	20	100	100
Seitz-1-hsto30	6	2400	1200	355	20	260	355	700	250	4	30	100	100
Seitz-1-hsto40	6	2400	1200	355	20	260	355	700	250	4	40	100	100
Seitz-1-hsto60	6	2400	1200	355	20	260	355	700	250	4	60	100	100
Seitz-1-hsto70	6	2400	1200	355	20	260	355	700	250	4	70	100	100
Seitz-1-hsto80	6	2400	1200	355	20	260	355	700	250	4	80	100	100
Seitz-1-hstw50	6	2400	1200	355	20	260	355	700	275	4	50	50	100
Seitz-1-hstw75	6	2400	1200	355	20	260	355	700	262.5	4	50	75	100
Seitz-1-hstw125	6	2400	1200	355	20	260	355	700	237.5	4	50	125	100

Specimen	t_w	a	h_w	f_{yw}	t_f	b_f	f_{yf}	s_s	b_l	t_{st}	$h_{st,o}$	$h_{st,w}$	b_{st}
Seitz-1-hstw150	6	2400	1200	355	20	260	355	700	225	4	50	150	100
Seitz-1-hstw175	6	2400	1200	355	20	260	355	700	212.5	4	50	175	100
Seitz-1-hstw200	6	2400	1200	355	20	260	355	700	200	4	50	200	100
Seitz-1-bl120	6	2400	1200	355	20	260	355	700	120	4	50	100	100
Seitz-1-bl160	6	2400	1200	355	20	260	355	700	160	4	50	100	100
Seitz-1-bl200	6	2400	1200	355	20	260	355	700	200	4	50	100	100
Seitz-1-bl240	6	2400	1200	355	20	260	355	700	240	4	50	100	100
Seitz-1-bl280	6	2400	1200	355	20	260	355	700	280	4	50	100	100
Seitz-1-bl320	6	2400	1200	355	20	260	355	700	320	4	50	100	100
Seitz-1-ss100	6	2400	1200	355	20	260	355	100	250	4	50	100	100
Seitz-1-ss200	6	2400	1200	355	20	260	355	200	250	4	50	100	100
Seitz-1-ss300	6	2400	1200	355	20	260	355	300	250	4	50	100	100
Seitz-1-ss400	6	2400	1200	355	20	260	355	400	250	4	50	100	100
Seitz-1-ss500	6	2400	1200	355	20	260	355	500	250	4	50	100	100
Seitz-1-ss600	6	2400	1200	355	20	260	355	600	250	4	50	100	100
Seitz-1-ss800	6	2400	1200	355	20	260	355	800	250	4	50	100	100
Seitz-1-ss900	6	2400	1200	355	20	260	355	900	250	4	50	100	100
Seitz-1-ss1000	6	2400	1200	355	20	260	355	1000	250	4	50	100	100
Seitz-1-ss1100	6	2400	1200	355	20	260	355	1100	250	4	50	100	100
Seitz-1-ss1200	6	2400	1200	355	20	260	355	1200	250	4	50	100	100
Seitz-1-tw3	3	2400	1200	355	20	260	355	700	250	4	50	100	100
Seitz-1-tw4	4	2400	1200	355	20	260	355	700	250	4	50	100	100
Seitz-1-tw5	5	2400	1200	355	20	260	355	700	250	4	50	100	100
Seitz-1-tw7	7	2400	1200	355	20	260	355	700	250	4	50	100	100
Seitz-1-tw8	8	2400	1200	355	20	260	355	700	250	4	50	100	100

Specimen	t_w	a	h_w	f_{yw}	t_f	b_f	f_{yf}	s_s	b_l	t_{st}	$h_{st,o}$	$h_{st,w}$	b_{st}
Seitz-2	6	2400	1200	355	20	260	355	700	250	4	50	100	100
Seitz-2-tst3	6	2400	1200	355	20	260	355	700	250.5	3	50	100	100
Seitz-2-tst8	6	2400	1200	355	20	260	355	700	248	8	50	100	100
Seitz-2-bst50	6	2400	1200	355	20	260	355	700	250	4	50	100	50
Seitz-2-bst150	6	2400	1200	355	20	260	355	700	250	4	50	100	150
Seitz-2-hsto20	6	2400	1200	355	20	260	355	700	250	4	20	100	100
Seitz-2-hsto80	6	2400	1200	355	20	260	355	700	250	4	80	100	100
Seitz-2-hstw50	6	2400	1200	355	20	260	355	700	275	4	50	50	100
Seitz-2-hstw200	6	2400	1200	355	20	260	355	700	200	4	50	200	100
Seitz-2-ss100	6	2400	1200	355	20	260	355	100	250	4	50	100	100
Seitz-2-ss1200	6	2400	1200	355	20	260	355	1200	250	4	50	100	100
Seitz-2-tw3	3	2400	1200	355	20	260	355	700	250	4	50	100	100
Seitz-2-tw8	8	2400	1200	355	20	260	355	700	250	4	50	100	100

Appendix B MATLAB script files

1 RunCalculations

```
%RunCalculations   Runs the calculations from the given dataset with
dimensions and properties.

    % Read the dataset with dimensions and properties
        T = readtable('Data\Data.xlsx', 'ReadVariableNames', true,
'ReadRowNames', true, 'PreserveVariableNames', true);

    % Review the rows, perform the calculations, and save the results

        % Read the size of the dataset
            Size = size(T);
            n = Size(1,1);

        % Perform the calculations row by row
            for k = 1 : n   % Loop each row
                % Read the parameters
                    tw   = T{k,1};
                    a    = T{k,2};
                    hw   = T{k,3};
                    fyw  = T{k,4};
                    tf   = T{k,5};
                    bf   = T{k,6};
                    fyf  = T{k,7};
                    ss   = T{k,8};
                    bl   = T{k,9};
                    tst  = T{k,10};
                    hsto = T{k,11};
                    hstw = T{k,12};
                    bst  = T{k,13};

                % Perform the calculations
                    if bl == 0  % Not stiffened
                        T{k,14} = GLJ_Unstiffened(tw, a, hw, fyw, tf, bf,
fyf, ss);
                        T(k,15) = {nan};    % Report as empty cell
                        T(k,16) = {nan};    % Report as empty cell
                    else        % Stiffened
                        Isl1 = calcIsl1(tw, fyw, tst, hsto, hstw, bst);
                        T{k,14} = GLJ(tw, a, hw, fyw, tf, bf, fyf, ss, bl,
Isl1);
                        T{k,15} = Davaine(tw, a, hw, fyw, tf, bf, fyf, ss,
bl, Isl1);
                        T{k,16} = GLM(tw, a, hw, fyw, tf, bf, fyf, ss, bl,
Isl1);
                    end
            end

        % Save the results
            R = T(1:n, 14:16);
            writetable(R, 'Data\Data.xlsx', 'WriteVariableNames', false,
'WriteRowNames', false, 'Range', 'O2');
```

2 calcIsl1

```
function [I] = calcIsl1(tw, fyw, tst, hsto, hstw, bst)
%calcIsl1 Calculates the second moment of area of a stiffener.

%% Parameters

    epsilon = sqrt(235/fyw);

%% Calculation

    if (hsto == 0 && hstw == 0) % Open section stiffener
        % Centre of gravity
            Ast = tst * bst;
            zst = tw + bst/2;
            Aweff = (2 * 15 * epsilon * tw + tst) * tw;
            zweff = tw/2;
            z = (Ast * zst + Aweff * zweff) / (Ast + Aweff);

        % Second moment of area
            Ist = tst * bst^3 / 12;
            Iweff = (2 * 15 * epsilon * tw + tst) * tw^3 / 12;
            I = Ist + Ast * (zst - z)^2 + Iweff + Aweff * (z - zweff)^2;

    else                        % Closed section stiffener
        % Centre of gravity
            h1 = hstw - (hstw - hsto) / 2;
            b1 = bst;
            h2 = hstw - 2 * tst - (hstw - 2 * tst - hsto - 2 * tst) / 2;
            b2 = bst - tst;

            Ast1 = h1 * b1;
            zst1 = tw + b1 / 2;
            Ast2 = h2 * b2;
            zst2 = tw + b2 / 2;

            aIn = 2 * (15 * epsilon * tw + tst);
            aOut = 2 * 15 * epsilon * tw;
            if aIn > hstw   % Physical distance check
                aIn = hstw;
            end

            Aweff = (aIn + aOut) * tw;
            zweff = tw/2;
            z = (Ast1 * zst1 - (Ast2 * zst2) + Aweff * zweff) / (Ast1 -
Ast2 + Aweff);

        % Second moment of area
            Ist1 = h1 * b1^3 / 12;
            Ist2 = h2 * b2^3 / 12;
            Iweff = (aIn + aOut) * tw^3 / 12;
            I = Ist1 + Ast1 * (zst1 - z)^2 - (Ist2 + Ast2 * (zst2 - z)^2) +
Iweff + Aweff * (z - zweff)^2;

    end
end
```

3 GLJ_Unstiffened

```
function [FRd] =  GLJ_Unstiffened(tw, a, hw, fyw, tf, bf, fyf, ss)
%GLJ_Unstiffened Patch loading resistance calculation according to EN1993-
1-5, developed by Graciano, Lagerqvist and Johannson, for unstiffened
girders.

%% Parameters

    % Universal parameters
        gammaM1 = 1.10;
        nuSteel = 0.3;
        E = 210 * 10^3; % MPa

%% Calculation

    % Effective loaded length
        m1 = (fyf * bf) / (fyw * tw);
        m2 = 0.02 * (hw / tf)^2;
        ly = ss + 2*tf*(1+sqrt(m1+m2));
        if(ly > a)
            ly = a;
        end

    % Buckling coefficient and buckling load
        kF = 6 + 2 * (hw / a)^2;
        Fcr = kF * pi^2 * E * tw ^3 / (12 * (1 - nuSteel^2) * hw);

    % Reduction factor
        lambdaF = sqrt(ly * tw * fyw / Fcr);
        if lambdaF <= 0.50
            m2 = 0;
            ly = ss + 2*tf*(1+sqrt(m1+m2));
            if(ly > a)
                ly = a;
            end
            lambdaF = sqrt(ly * tw * fyw / Fcr);
            if lambdaF > 0.50
                disp('Error: Lambda value is not in range.')
            end
        end
        chiF = 0.5 / lambdaF;
        if chiF > 1
            chiF = 1;
        end

    % Final patch loading calculation
        FRd = (chiF * ly * fyw * tw / gammaM1) * 10^(-3);    % kN

end
```

4 GLJ

```
function [FRd] =  GLJ(tw, a, hw, fyw, tf, bf, fyf, ss, bl, Isl1)
%GLJ Patch loading resistance calculation according to EN1993-1-5,
developed by Graciano, Lagerqvist and Johannson.

%% Parameters

    % Universal parameters
        gammaM1 = 1.10;
        nuSteel = 0.3;
        E = 210 * 10^3; % MPa

    % Specific parameters
        alphaF0 = 0.75;
        lambdaF0 = 0.50;

%% Calculation

    % Effective loaded length
        m1 = (fyf * bf) / (fyw * tw);
        if lambdaF0 <= 0.50
            m2 = 0;
        else
            m2 = 0.02 * (hw / tf)^2;
        end
        ly = ss + 2*tf*(1+sqrt(m1+m2));
        if(ly > a)
            ly = a;
        end

    % Buckling coefficient and buckling load
        gammaS = 10.9 * Isl1 / (hw * tw^3);
        gammaSCon = 13 * (a / hw)^3 + 210 * (0.3 - bl / a);
        if gammaS > gammaSCon
            gammaS = gammaSCon;
        end
        kF = 6 + 2 * (hw / a)^2 + (5.44 * bl /a - 0.21) * sqrt(gammaS);
        Fcr = kF * pi^2 * E * tw ^3 / (12 * (1 - nuSteel^2) * hw);

    % Reduction factor
        lambdaF = sqrt(ly * tw * fyw / Fcr);
        phiF = 1/2 * (1 + alphaF0 * (lambdaF - lambdaF0) + lambdaF);
        chiF = 1 / (phiF + sqrt(phiF^2 - lambdaF));
        if chiF > 1
            chiF = 1;
        end

    % Final patch loading calculation
        FRd = (chiF * ly * fyw * tw / gammaM1) * 10^(-3);    % kN

end
```

5 Davaine

```
function [FRd] =  Davaine(tw, a, hw, fyw, tf, bf, fyf, ss, bl, Isl1)
%DAVAINE Patch loading resistance calculation according to Davaine.

%% Parameters

    % Universal parameters
        gammaM1 = 1.10;
        nuSteel = 0.3;
        E = 210 * 10^3; % MPa

    % Specific parameters
        alphaF0 = 0.21;
        lambdaF0 = 0.80;
        m2 = 0;

%% Calculation

    % Effective loaded length
        m1 = (fyf * bf) / (fyw * tw);
        ly = ss + 2*tf*(1+sqrt(m1+m2));
        if(ly > a)
            ly = a;
        end

    % Buckling coefficient and buckling load
        gammaS = 10.9 * Isl1 / (hw * tw^3);
        gammaSCon = 13 * (a / hw)^3 + 210 * (0.3 - bl / a);
        if gammaS > gammaSCon
            gammaS = gammaSCon;
        end
        kF1 = 6 + 2 * (hw / a)^2 + (5.44 * bl / a - 0.21) * sqrt(gammaS);
        Fcr1 = kF1 * pi^2 * E * tw ^3 / (12 * (1 - nuSteel^2) * hw);
        kF2 = (0.8 * (ss + 2*tf) / a + 0.6) * (a / bl )^((0.6 * (ss + 2*tf)
/ a + 0.5));
        Fcr2 = kF2 * pi^2 * E * tw ^3 / (12 * (1 - nuSteel^2) * bl);
        Fcr = Fcr1 * Fcr2 / (Fcr1 + Fcr2);

    % Reduction factor
        lambdaF = sqrt(ly * tw * fyw / Fcr);
        phiF = 1/2 * (1 + alphaF0 * (lambdaF - lambdaF0) + lambdaF);
        chiF = 1 / (phiF + sqrt(phiF^2 - lambdaF));
        if chiF > 1
            chiF = 1;
        end

    % Final patch loading calculation
        FRd = (chiF * ly * fyw * tw / gammaM1) * 10^(-3);    % kN

end
```

6 GLM

```
function [FRd] =  GLM(tw, a, hw, fyw, tf, bf, fyf, ss, bl, Isl1)
%GLM Patch loading resistance calculation according to Graciano, Lagerqvist
and Mendes.

%% Parameters

    % Universal parameters
        gammaM1 = 1.10;
        nuSteel = 0.3;
        E = 210 * 10^3; % MPa

    % Specific parameters
        alphaF0 = 0.75;
        lambdaF0 = 0.50;

%% Calculation

    % Effective loaded length
        m1 = (fyf * bf) / (fyw * tw);
        if lambdaF0 <= 0.50
            m2 = 0;
        else
            m2 = 0.02 * (hw / tf)^2;
        end
        ly = ss + 2*tf*(1+sqrt(m1+m2));
        if(ly > a)
            ly = a;
        end

    % Buckling coefficient and buckling load
        gammaS = 10.9 * Isl1 / (hw * tw^3);
        gammaSCon = 13 * (a / hw)^3 + 210 * (0.3 - bl / a);
        if gammaS > gammaSCon
            gammaS = gammaSCon;
        end
        ksl = -1.87 + 36.94 * bl / hw - 62.86 * (bl / hw)^2 - 8.09 * ss / a
+ 16.38 * (ss / a)^2 - 0.0036 * gammaS + 0.44 * tf / tw + 30.95 * bl / hw *
ss / a + 0.031 * bl / hw * gammaS + 0.0035 * ss / a * gammaS;
        kF = 6 + 2 * (hw / a)^2 + ksl;
        Fcr = kF * pi^2 * E * tw ^3 / (12 * (1 - nuSteel^2) * hw);

    % Reduction factor
        lambdaF = sqrt(ly * tw * fyw / Fcr);
        phiF = 1/2 * (1 + alphaF0 * (lambdaF - lambdaF0) + lambdaF);
        chiF = 1 / (phiF + sqrt(phiF^2 - lambdaF));
        if chiF > 1
            chiF = 1;
        end

    % Final patch loading calculation
        FRd = (chiF * ly * fyw * tw / gammaM1) * 10^(-3);    % kN

end
```

Appendix C Exact parameters for the Newton-Raphson approach

Both the control nodes (*Point de contrôle*) and the multiplier for the first passage (*Valeur 1er pas (CREM)*) may vary per model.

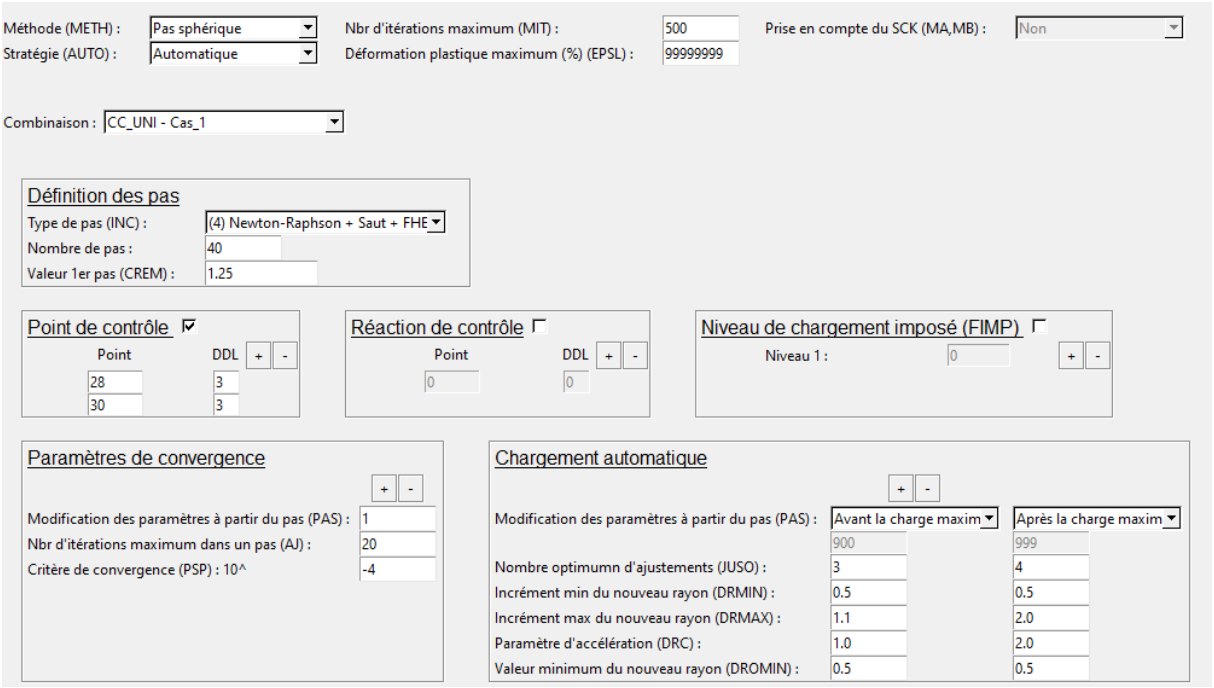

Figure 61: Screenshot of FINELG's "Paramètres Calcul non-linéaire" window [15].

Appendix D Results of analysed models

Table 7: List of results of the analysed models.

Specimen	$F_{Rd,GLJ}$	$F_{Rd,Davaine}$	$F_{Rd,GLM}$	$F_{Rd,FEM}$	Failure mode
Kövesdi-1	164	183	187	194	local - even
Kövesdi-1-tst3	162	182	187	193	local - even
Kövesdi-1-tst5	166	185	187	195	local - even
Kövesdi-1-tst6	167	186	187	196	local - even
Kövesdi-1-tst7	168	187	188	197	local - even
Kövesdi-1-tst8	169	188	188	198	local - even
Kövesdi-1-bst25	154	176	187	192	local - even
Kövesdi-1-bst35	160	181	187	193	local - even
Kövesdi-1-bst45	167	186	188	194	local - even
Kövesdi-1-bst55	175	190	189	195	local - even
Kövesdi-1-bst65	182	194	190	195	local - even
Kövesdi-1-bst75	189	198	191	195	local - even
Kövesdi-1-bl50	147	202	160	212	local - lower subpanel
Kövesdi-1-bl75	160	206	174	208	local - lower subpanel
Kövesdi-1-bl100	175	204	184	201	local - lower subpanel
Kövesdi-1-bl125	190	198	192	194	local - even
Kövesdi-1-bl150	201	187	196	214	local - upper subpanel
Kövesdi-1-ss50	121	126	135	135	local - even
Kövesdi-1-ss100	137	146	154	152	local - even
Kövesdi-1-ss150	151	165	171	167	local - even
Kövesdi-1-ss250	176	201	204	218	local - even
Kövesdi-1-ss300	187	218	221	236	local - even
Kövesdi-1-ss350	197	235	238	259	local - even
Kövesdi-1-tw3	100	109	112	118	local - even
Kövesdi-1-tw5	241	275	281	280	local - even
Kövesdi-1-tw6	332	384	390	370	local - upper subpanel
Kövesdi-1-tw7	435	511	514	459	local - upper subpanel
Kövesdi-1-tw8	550	653	651	549	local - upper subpanel
Kövesdi-2	164	183	187	212	local - upper subpanel
Kövesdi-2-tst3	162	182	187	212	interactive
Kövesdi-2-tst8	169	188	188	215	interactive
Kövesdi-2-bst25	154	176	187	209	interactive
Kövesdi-2-bst75	189	198	191	214	local - upper subpanel
Kövesdi-2-ss50	121	126	135	138	local - upper subpanel
Kövesdi-2-ss350	197	235	238	311	interactive
Kövesdi-2-tw3	100	109	112	128	local - upper subpanel
Kövesdi-2-tw8	550	653	651	559	global

Specimen	$F_{Rd,GLJ}$	$F_{Rd,Davaine}$	$F_{Rd,GLM}$	$F_{Rd,FEM}$	**Failure mode**
Kövesdi-3	164	183	187	207	local - upper subpanel
Kövesdi-3-tst3	162	182	187	206	local - upper subpanel
Kövesdi-3-tst8	169	188	188	211	local - upper subpanel
Kövesdi-3-bst25	154	176	187	202	local - upper subpanel
Kövesdi-3-bst75	189	198	191	210	local - upper subpanel
Kövesdi-3-ss50	121	126	135	137	local - upper subpanel
Kövesdi-3-ss350	197	235	238	291	local - upper subpanel
Kövesdi-3-tw3	100	109	112	124	local - upper subpanel
Kövesdi-3-tw8	550	653	651	557	global
Seitz-1	442	523	486	683	local - lower subpanel
Seitz-1-tst3	433	515	485	675	local - lower subpanel
Seitz-1-tst5	449	528	488	686	local - lower subpanel
Seitz-1-tst6	454	533	489	689	local - lower subpanel
Seitz-1-tst7	454	533	489	691	local - lower subpanel
Seitz-1-tst8	453	533	488	692	local - lower subpanel
Seitz-1-bst50	401	489	480	612	local - upper subpanel
Seitz-1-bst60	410	496	481	636	local - upper subpanel
Seitz-1-bst70	418	503	482	693	local - even
Seitz-1-bst80	426	510	484	697	local - lower subpanel
Seitz-1-bst90	434	516	485	696	local - lower subpanel
Seitz-1-bst110	450	528	488	694	local - lower subpanel
Seitz-1-bst120	455	532	489	692	local - lower subpanel
Seitz-1-bst130	455	532	489	696	local - lower subpanel
Seitz-1-bst140	455	532	489	698	local - lower subpanel
Seitz-1-bst150	455	532	489	701	local - lower subpanel
Seitz-1-hsto20	435	517	485	670	local - lower subpanel
Seitz-1-hsto30	437	519	486	675	local - lower subpanel
Seitz-1-hsto40	440	521	486	679	local - lower subpanel
Seitz-1-hsto60	444	524	487	683	local - lower subpanel
Seitz-1-hsto70	446	526	487	687	local - lower subpanel
Seitz-1-hsto80	448	527	488	688	local - lower subpanel
Seitz-1-hstw50	439	505	492	647	local - lower subpanel
Seitz-1-hstw75	441	514	490	668	local - lower subpanel
Seitz-1-hstw125	441	529	483	705	local - lower subpanel
Seitz-1-hstw150	439	535	479	713	local - lower subpanel
Seitz-1-hstw175	434	538	473	738	local - lower subpanel
Seitz-1-hstw200	426	539	468	753	local - lower subpanel
Seitz-1-bl120	371	514	419	912	local - lower subpanel
Seitz-1-bl160	394	526	444	846	local - lower subpanel
Seitz-1-bl200	416	529	465	763	local - lower subpanel
Seitz-1-bl240	437	525	483	700	local - lower subpanel
Seitz-1-bl280	457	515	497	638	local - upper subpanel

Specimen	$F_{Rd,GLJ}$	$F_{Rd,Davaine}$	$F_{Rd,GLM}$	$F_{Rd,FEM}$	**Failure mode**
Seitz-1-bl320	476	501	508	692	local - upper subpanel
Seitz-1-ss100	277	291	292	354	local - upper subpanel
Seitz-1-ss200	311	334	328	379	local - even
Seitz-1-ss300	341	374	361	421	local - even
Seitz-1-ss400	369	413	393	481	local - even
Seitz-1-ss500	395	451	424	549	local - even
Seitz-1-ss600	419	487	455	612	local - even
Seitz-1-ss800	464	557	518	751	local - lower subpanel
Seitz-1-ss900	485	590	550	816	local - lower subpanel
Seitz-1-ss1000	505	623	583	881	local - lower subpanel
Seitz-1-ss1100	524	654	617	915	local - lower subpanel
Seitz-1-ss1200	542	685	653	969	local - lower subpanel
Seitz-1-tw3	121	140	137	171	local - even
Seitz-1-tw4	209	244	232	303	local - even
Seitz-1-tw5	321	374	349	478	local - lower subpanel
Seitz-1-tw7	574	688	644	907	local - lower subpanel
Seitz-1-tw8	722	875	824	1132	local - lower subpanel
Seitz-2	442	523	486	1121	interactive
Seitz-2-tst3	433	515	485	1091	interactive
Seitz-2-tst8	453	533	488	1180	interactive
Seitz-2-bst50	401	489	480	800	interactive
Seitz-2-bst150	455	532	489	1201	local - upper subpanel
Seitz-2-hsto20	435	517	485	1075	interactive
Seitz-2-hsto80	448	527	488	1144	interactive
Seitz-2-hstw50	439	505	492	1036	interactive
Seitz-2-hstw200	426	539	468	1250	interactive
Seitz-2-ss100	277	291	292	511	interactive
Seitz-2-ss1200	542	685	653	1612	interactive
Seitz-2-tw3	121	140	137	250	local - upper subpanel
Seitz-2-tw8	722	875	824	1699	interactive

Appendix E Select deformation and load-deformation diagrams

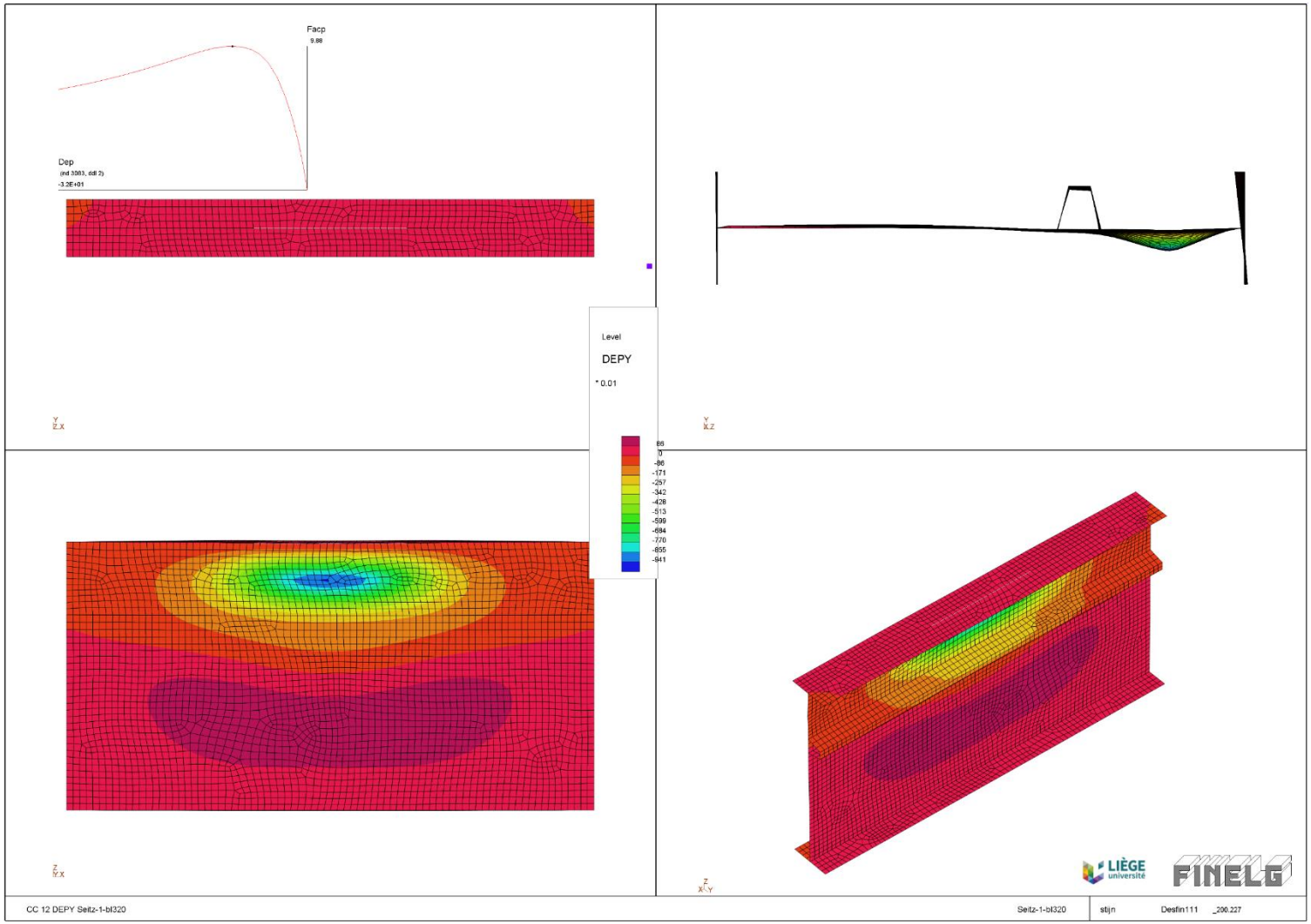

Figure 62: Local buckling; failure of the upper subpanel; Seitz-1-bl320 [15].

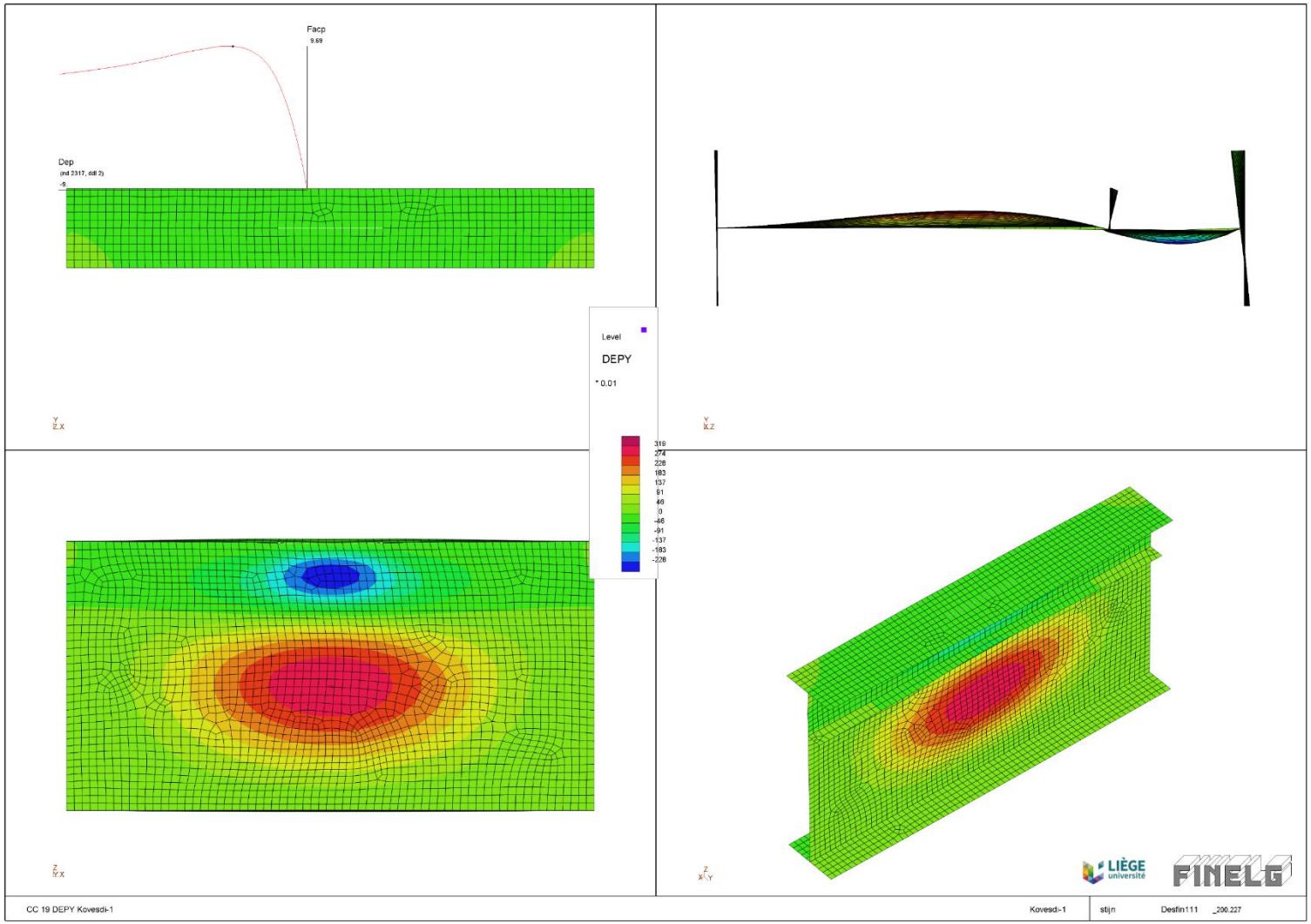

Figure 63: Local buckling; about even failure; Kövesdi-1 [15].

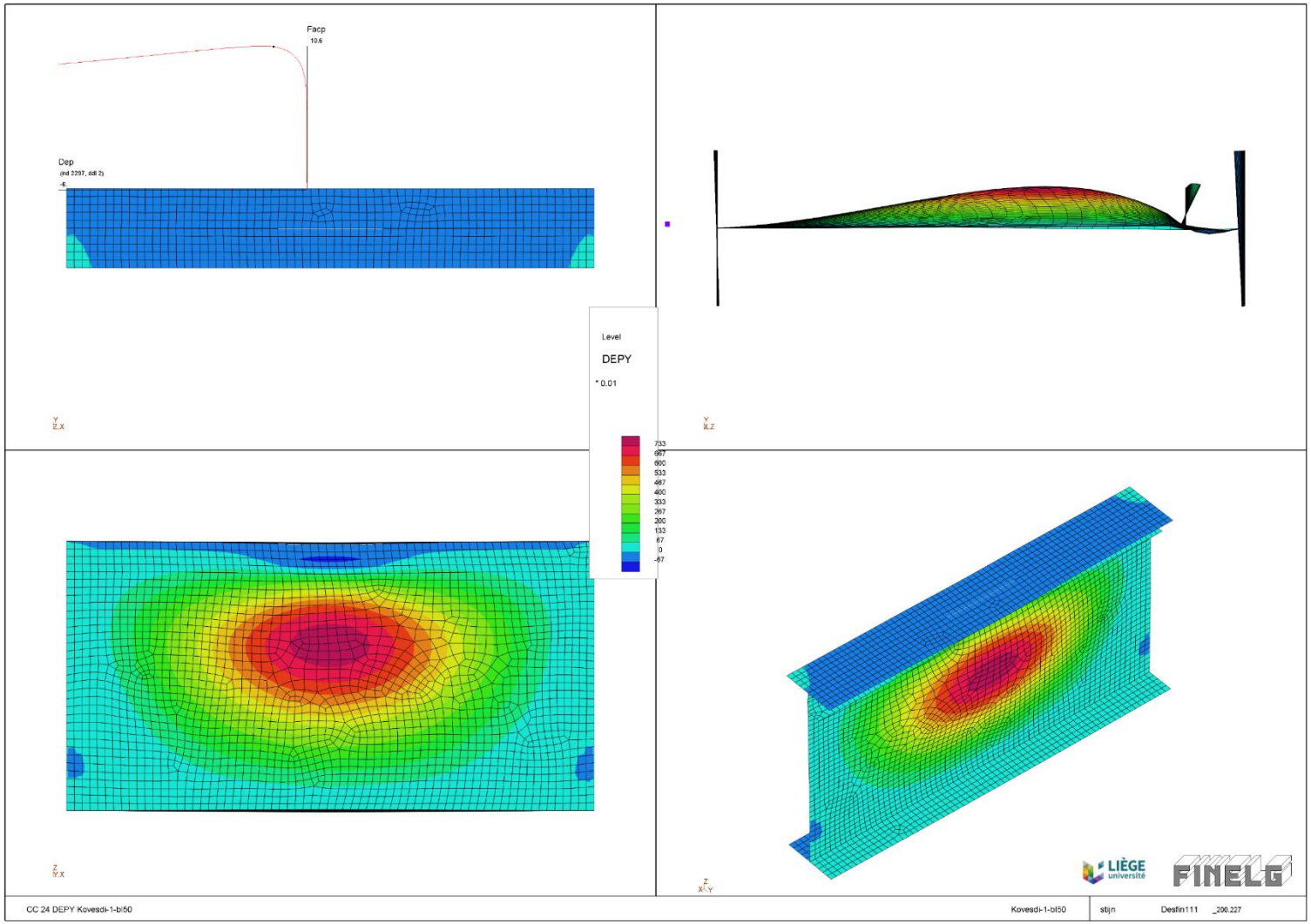

Figure 64: Local buckling; failure of the lower subpanel; Kövesdi-1-bl50 [15].

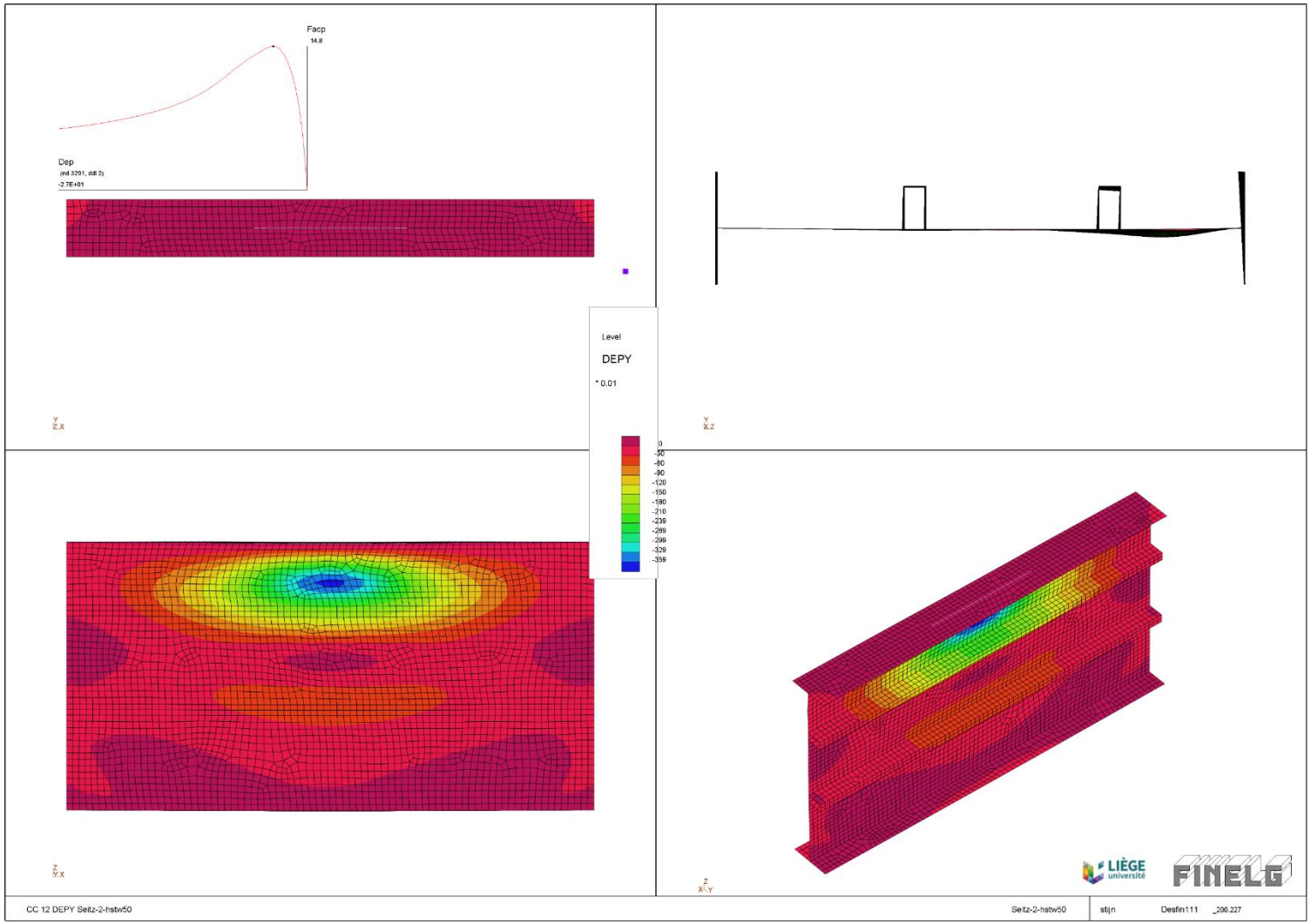

Figure 65: Interactive buckling; Seitz-2-hstw50 [15].

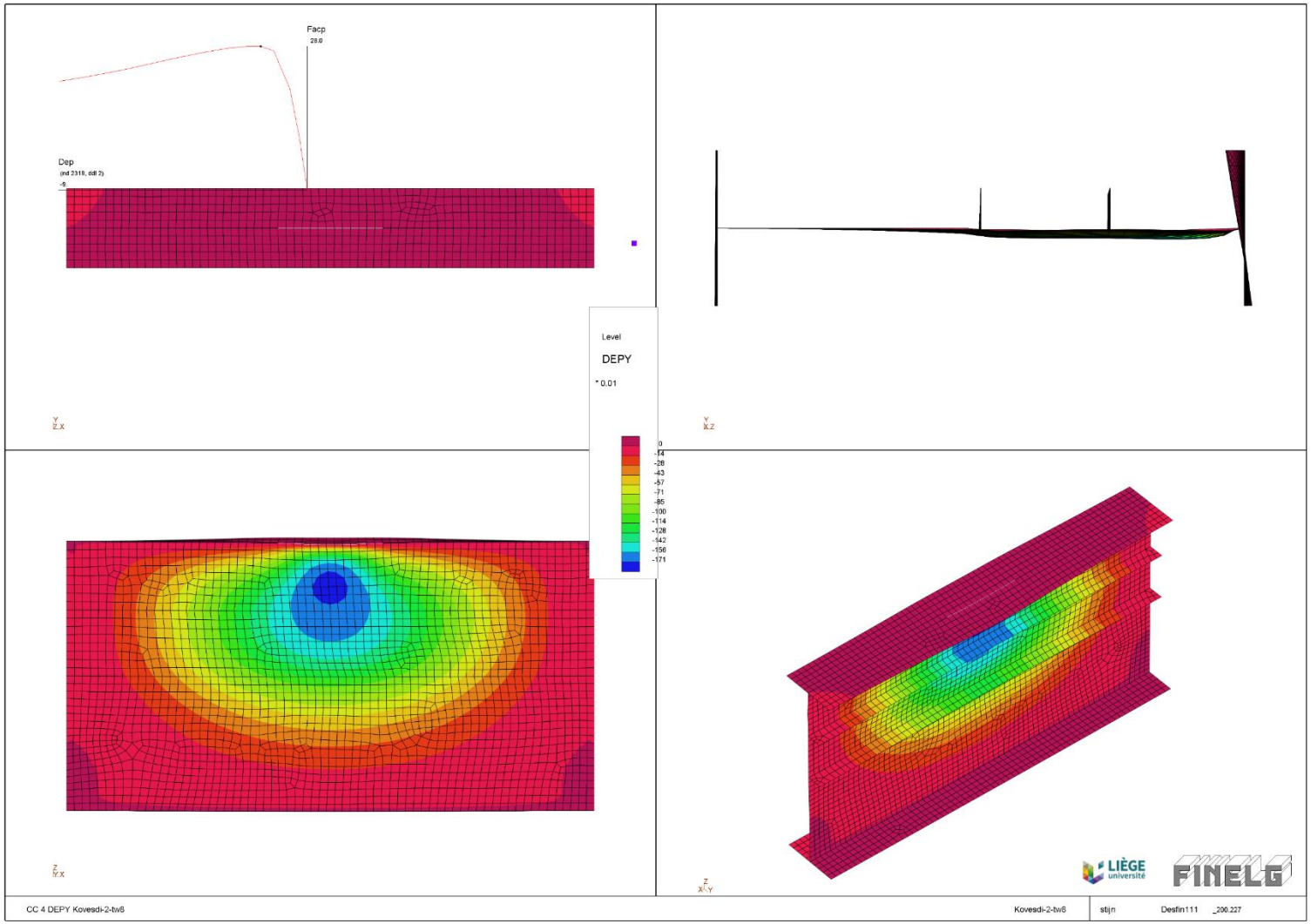

Figure 66: Global web buckling; Kövesdi-2-tw8 [15].